*Earth-Science Reviews*, 26 (1989) 163–189
Elsevier Science Publishers B.V., Amsterdam—Printed in The Netherlands





# Modelling the General Circulation of Shelf Seas by 3D $k-\epsilon$ Models



JACQUES C.J. NIHOUL, ERIC DELEERSNIJDER and SALIM DJENIDI



ABSTRACT

Nihoul, J.C.J., Deleersnijder, E. and Djenidi, S., 1989. Modelling the general circulation of shelf seas by 3D $k-\epsilon$ models. Earth-Sci. Rev., 26: 163–189.

One examines the modifications which must be made—and the limitations which must be set—to classical $k-\epsilon$ models to extend their application to the simulation of marine mesoscale, synopticscale and macroscale processes which compose the weather-like and general circulations of the sea.

The case of the general circulation—for which sub-grid scale fluctuations include such semi-organized motions as tides and storm surges—is discussed in more detail.

A 3D $k-\epsilon$ model appropriate to the study of the general circulation in a shallow stratified sea is presented and illustrated with the results of a simulation of the general summer circulation in the Northern Bering Sea, made in the scope of the NSF ISHTAR ("Inner Shelf Transfer and Recycling") Program.

## INTRODUCTION

The computation of the mean properties of turbulent flows by 2D and 3D mathematical models, with second order closure at the turbulent kinetic energy $k$ and turbulent energy dissipation rate $\epsilon$, has a long history of successes and partial failures and is well documented in the specialized literature (e.g., Lumley, 1978; Rodi, 1980).

The application of these models to geohydrodynamic problems, and in particular the simulation of current fields and transports in oceans, shelf seas and estuaries, has been the subject of considerable developments in the recent years (e.g., Blumberg and Mellor, 1980, 1985; Nihoul and Djenidi, 1987; Rodi, 1987).

The extension of three-dimensional $k-\epsilon$ models to geophysical flows, however, is not as obvious as one would like.

While, in simple laboratory experiments, the distinction between the "mean flow" and the superimposed "turbulent fluctuations" is completely unambiguous, geophysical systems are characterized by a continuum of interacting motions of all time scales and length scales. Each particular process must be studied in the frame of its "spectral window" embedded in the slowly varying environment of the larger scales and blurred by the (non-linear) diffusing effect of "sub-window" or "sub-grid" scale processes, showing many of the characteristics of turbulence (e.g., Monin et al., 1977; Nihoul, 1980; Table I).

Whether, for a specific spectral window, sub-grid scale fluctuations are sufficiently similar to three-dimensional turbulence to allow the type of parameterization which is used in $k-\epsilon$ models and how much $k-\epsilon$ schemes may have to be modified to accommodate non-negligible differences, are the questions one must ask and answer before expensive geohydrodynamic simulations are undertaken.

The purpose of this paper is to examine the modifications which must be made—and the

0012-8252/89/$9.45 

limitations which must be set—to the original $k-\epsilon$ model, devised for simple turbulent flows, to extend its application to the simulation of marine mesoscale, synopticscale and macroscale processes which compose the weather-like and general circulations of the sea.

The case of the general circulation, for which sub-window scale fluctuations include such semi-organized motions as tides, and storm surges, is discussed in more detail.

A three-dimensional, non-linear, $k-\epsilon$ model appropriate to the study of the general circulation in shallow stratified seas and developed at the GeoHydrodynamics and Environment Research Laboratory of the University of Liège (GHER) is presented and illustrated with the results of a simulation of the general circulation in the Northern Bering Sea, in "climatological" summer conditions, made in the scope of the NSF ISHTAR ("Inner Shelf Transfer and Recycling") Program.

## 1 ESSENTIALS OF THE $k-\epsilon$ MODEL

The geohydrodynamic or "Boussinesq" equations may be written, for the sea (e.g.,

---

Jacques C.J. Nihoul, born June 6, 1937, Engineer (Liège University, Belgium) 1960, Master of Science in Mathematics (MIT, U.S.A.) 1961, Ph. D. in Applied Mathematics and Theoretical Physics (University of Cambridge, U.K.) 1965, Professor of Geophysical Fluid Dynamics in the Universities of Liège and Louvain.

Eric Deleersnijder, born April 25, 1961, Engineer (Liège University, Belgium) 1984, Research Assistant, National Fund for Scientific Research, Belgium.

Salim Djenidi, born August 11, 1954, Engineer (Liège University, Belgium) 1979, Bachelor in Oceanography (Liège University, Belgium) 1980, Ph.D. in Applied Sciences (Liège University, Belgium) 1987, Principal Research Assistant, Liège University, Belgium.

TABLE I

Schematic representation of marine variability

| Time scale | Frequency ($s^{-1}$) | Spectral windows (highlighted processes) | Smaller scale fluctuations (filtered-out processes) |
|---|---|---|---|
| 1 s | 1 | *Microscale processes*<br>3D "eddy" turbulence<br>(+surface waves) | Molecular diffusion |
| 1 min | $10^{-2}$ | *Mesialscale processes*<br>Internal waves<br>Vertical microstructure<br>"Bliny" *1 inhibited turbulence | Eddy turbulence |
| 1h | $10^{-4}$ | *Mesoscale processes*<br>Inertial oscillations | "Bliny turbulence" |
| 1 day | $10^{-5}$ | Tides, storm surges<br>Diurnal variations | |
| 1 week | $10^{-6}$ | *Synopticscale processes*<br>Frontal currents<br>Meanders, "rossby" *2 turbulence | Mesoscale variability |
| 1 month | $10^{-7}$ | *Seasonalscale processes* | "Rossby turbulence" |
| 1 year | $10^{-8}$ | *Globalscale processes*<br>Climatic processes | Seasonal variability |
| | | *(Paleo)climaticscale processes* | |

*1 A "bliny" (from the Russian blini) is a pancake-shaped eddy contributing to an energy cascade to smaller scales via epidermic instabilities and internal waves.

*2 A "rossby" (from the scientist Rossby) is a pseudo-two-dimensional eddy column of scale of the order of the Rossby radius of deformation.

Nihoul, 1977a):

$$\nabla \cdot \boldsymbol{v} = 0 \tag{1}$$

$$\frac{\partial \boldsymbol{v}}{\partial t} + \nabla \cdot (\boldsymbol{v}\,\boldsymbol{v}) + 2\boldsymbol{\Omega} \wedge \boldsymbol{v} = -\nabla\gamma + \boldsymbol{b} - \nabla \cdot \boldsymbol{\Phi}^{v} \tag{2}$$

$$\boldsymbol{b} = b\boldsymbol{e}_3; \quad b = -g\frac{\rho - \rho_0}{\rho_0} = b(\theta, \sigma) \tag{3}; (4)$$

$$\frac{\partial \theta}{\partial t} + \nabla \cdot (\boldsymbol{v}\theta) = -\nabla \cdot \boldsymbol{\phi}^{\theta} \tag{5}$$

$$\frac{\partial \sigma}{\partial t} + \nabla \cdot (\boldsymbol{v}\sigma) = -\nabla \cdot \boldsymbol{\phi}^{\sigma} \tag{6}$$

where:

$$\nabla = \boldsymbol{e}_1\frac{\partial}{\partial x_1} + \boldsymbol{e}_2\frac{\partial}{\partial x_2} + \boldsymbol{e}_3\frac{\partial}{\partial x_3}$$

$$\gamma = \frac{p}{\rho_0} + gx_3 + \xi \tag{7}$$

$\boldsymbol{v}$ is the velocity vector, $\boldsymbol{\Omega}$ the rotation vector of the earth, $b$ the buoyancy, $\theta$ the temperature, $\sigma$ the salinity, $\rho$ the density of sea water and $\rho_0$ a constant reference value, $g$ the acceleration of gravity, $p$ the pressure, $\xi$ the tidal potential, $\boldsymbol{\Phi}^{v}$, $\boldsymbol{\phi}^{\theta}$ and $\boldsymbol{\phi}^{\sigma}$, respectively, the molecular fluxes of momentum, heat and salt.

For simplicity, it has been assumed that heat and salt production is essentially due to radiation, heat and water exchanges at the air–sea interface and may be approximated by boundary sources taken into account in the formulation of the boundary conditions.

The equations for $\theta$ and $\sigma$ can be com-

bined, using the empirical state equation $b = b(\theta, \sigma)$, into a single equation for $b$ i.e. (e.g., Nihoul, 1977a):

$$\frac{\partial b}{\partial t} + \nabla \cdot (vb) = -\nabla \cdot \phi^b \tag{8}$$

where $\phi^b$ is the appropriate molecular flux of buoyancy.

To keep the following discussion in a simple framework, eq. 8 will be used in place of eqs. 5 and 6. The extension to a more complicated system where temperature and salinity must be determined separately is conceptually trivial.

Furthermore, it will be shown that the formulation is actually appropriate for the general circulation models one is mainly interested in.

The state variables are now $v$, $b$ and $p$. As such, however, they are not suitable to the description of the system. Observations in geophysical fluids reveal indeed random fluctuations and two instrumental records, made in exactly the same conditions—although qualitatively similar—cannot be superposed. Only the ensemble average of a large number of recordings made in identical conditions appears to be reproducible. These ensemble averages are the appropriate state variables for mathematical modelling.

The corresponding evolution equations can be derived from eqs. 1–8 in a simple way as follows: each state variable is regarded as a function of time $t$, space $x_1$, $x_2$, $x_3$ and a parameter $\delta$ chosen at random. The evolution equations of the model are obtained by averaging eqs. 1–8 over all values of $\delta$. The resulting equations are (e.g., Nihoul, 1977a):

$$\nabla \cdot \boldsymbol{u} = 0 \tag{9}$$

$$\frac{\partial \boldsymbol{u}}{\partial t} + \nabla \cdot (\boldsymbol{uu}) + 2\Omega \wedge \boldsymbol{u} = -\nabla q + \boldsymbol{a} - \nabla \cdot \tilde{\Phi}^u \tag{10}$$

$$\frac{\partial a}{\partial t} + \nabla \cdot (\boldsymbol{u}a) = -\nabla \cdot \tilde{\phi}^a \tag{11}$$

$$\boldsymbol{a} = a\boldsymbol{e}_3 \tag{12}$$

where, $\langle\ \rangle$ denoting an ensemble average,

$$\boldsymbol{u} = \langle \boldsymbol{v} \rangle; \quad \boldsymbol{v} = \boldsymbol{u} + \boldsymbol{w}; \quad \langle \boldsymbol{w} \rangle = 0$$

$$q = \langle \gamma \rangle; \quad \gamma = q + r; \quad \langle r \rangle = 0$$

$$a = \langle b \rangle; \quad b = a + c; \quad \langle c \rangle = 0$$

$$\tilde{\Phi}^u = \langle \Phi^u \rangle + \langle \boldsymbol{ww} \rangle \sim \langle \boldsymbol{ww} \rangle \tag{13}$$

$$\tilde{\phi}^a = \langle \phi^b \rangle + \langle \boldsymbol{w}c \rangle \sim \langle \boldsymbol{w}c \rangle \tag{14}$$

taking into account that molecular fluxes are much smaller than the "turbulent" fluxes $\langle \boldsymbol{ww} \rangle$ and $\langle \boldsymbol{w}c \rangle$.

To solve the system of eqs. 9–14, one must find expressions of the turbulent fluxes in terms of the mean variables. The parameterization of the fluxes is based on the following general understanding of turbulence (e.g., Nihoul, 1977a):

(i) The cogent activity of turbulent fluctuations is the transfer of energy, via an "eddy cascade" from the larger scales (where turbulence extracts energy from the mean flow) to the smaller scales (where energy is dissipated by viscosity).

(ii) The viscous sink is characterized by a length scale $l_v \sim \epsilon^{-1/4}\nu^{3/4}$, a velocity scale $u_v \sim \epsilon^{1/4}\nu^{1/4}$ and a "Reynolds number" $R_v \sim (u_v l_v)/\nu \sim 1$, where $\epsilon$ denotes the turbulent energy dissipation rate:

$$\epsilon = \nu \langle \nabla \boldsymbol{w} : \nabla \boldsymbol{w} \rangle \tag{15}$$

and where $\nu$ is the "kinematic viscosity".

(iii) The global effect of the turbulent fluctuations is analogous to molecular diffusion—with a much greater efficiency—and the turbulent fluxes may be parameterized, on the Fourier-Fick-Onsager model of molecular fluxes, in terms of the gradients of the mean state variables, i.e.:

$$\tilde{\Phi}^u \sim \langle \boldsymbol{ww} \rangle = -\tilde{\nu} \nabla \boldsymbol{u} \tag{16}$$

$$\tilde{\phi}^a \sim \langle \boldsymbol{w}c \rangle = -\tilde{\nu}^a \nabla a \tag{17}$$

and similar expressions for other turbulent fluxes. (In eqs. 16 and 17, $\tilde{\nu}$ and $\tilde{\nu}^a$ are the turbulent or "eddy" diffusivities for momentum and buoyancy; $\tilde{\nu}$ is thus the turbulent equivalent of the molecular viscosity $\nu$.)

(iv) The introduction of eddy diffusivities is tantamount to cutting off the energy cascade

and introducing, at the "outer scale" $l_m$ of turbulence where energy is extracted from the mean flow, an equivalent "eddy viscous" sink representing the cumulated effect of the energy cascade and the subsequent energy dissipation in the smaller scales, with the requirements that $l_m \sim \epsilon^{-1/4}\tilde{\nu}^{3/4}$, $u_m \sim \epsilon^{1/4}\tilde{\nu}^{1/4}$, $R_m = (u_m l_m)/\tilde{\nu} \sim 1$.

Taking into account the rapid decrease of the turbulent kinetic energy spectrum outside the range of the "energy containing eddies" at scale $l_m$ (e.g., Nihoul, 1977a), one may argue that $\frac{1}{2}u_m^2$ represents the essential part of the total turbulent kinetic energy (per unit mass):

$$k = \tfrac{1}{2}\langle \boldsymbol{w} \cdot \boldsymbol{w} \rangle \tag{18}$$

and write:

$$u_m = \alpha k^{\frac{1}{2}} \tag{19}$$

where $\alpha$ is an empirical coefficient, presumably of order 1.

Combining the expressions of $l_m$, $u_m$ and $R_m$, one obtains:

$$\tilde{\nu} = \alpha l_m k^{\frac{1}{2}} \tag{20}$$

$$\epsilon = \alpha^4 k^2 \tilde{\nu}^{-1} \tag{21}$$

An equation for the turbulent kinetic energy $k$ is readily obtained from eqs. 2 and 10. Subtracting eq. 10 from eq. 2, one gets an equation for $\boldsymbol{w}$. The scalar product of this equation by $\boldsymbol{w}$ gives (e.g., Nihoul, 1977a):

$$\frac{\partial k}{\partial t} + \nabla \cdot (\boldsymbol{u}k) = Q^k - \nabla \cdot \tilde{\boldsymbol{\phi}}^k \tag{22}$$

where:

$$Q^k = -\langle \boldsymbol{w}\boldsymbol{w} \rangle : \nabla \boldsymbol{u} + \langle c w_3 \rangle - \epsilon \tag{23}$$

is the rate of production–destruction of turbulent kinetic energy and:

$$\tilde{\boldsymbol{\phi}}^k = -\tilde{\nu}^k \nabla k \tag{24}$$

is the corresponding turbulent flux ($\tilde{\nu}^k$ is the turbulent diffusivity for $k$).

The system of eqs. 9–24 is closed if one can provide an (empirical algebraic or differential) equation for $l_m$ or $\epsilon$.

In many circumstances, in shallow shelf seas, sound empirical formulas are available for $l_m$, deduced from observations. In other cases, an additional evolution equation is needed.

An equation for $\epsilon$ can be derived from the equation for $\boldsymbol{w}$, in much the same way as the equation for $k$ (e.g., Lumley, 1978; Blumberg and Mellor, 1985; Nihoul and Djenidi, 1987; Rodi, 1987). This equation has the form:

$$\frac{\partial \epsilon}{\partial t} + \nabla \cdot (\boldsymbol{u}\epsilon) = Q^\epsilon - \nabla \cdot \tilde{\boldsymbol{\phi}}^\epsilon \tag{25}$$

where $Q^\epsilon$ and $\tilde{\boldsymbol{\phi}}^\epsilon$ are respectively the rate of production and the turbulent flux of the energy dissipation rate.

In the eddy diffusivity approximation, $\tilde{\boldsymbol{\phi}}^\epsilon$ can be written:

$$\tilde{\boldsymbol{\phi}}^\epsilon = -\tilde{\nu}^\epsilon \nabla \epsilon \tag{26}$$

The rate of production $Q^\epsilon$ must be expressed in terms of the mean properties of the turbulent field and this is one of the main difficulties of $k$–$\epsilon$ models.

The parameterization is not as obvious as for other terms (like $Q^k$, for instance) and often simple formulas cannot be obtained without rather limiting hypotheses on the characteristics of the turbulent fluctuations.

Widely-used expressions of $Q^\epsilon$ have the form of linear combinations of the three components of $Q^k$, i.e., factorizing a scaling factor $\epsilon k^{-1}$,

$$Q^\epsilon = \frac{\epsilon}{k}\left[ -\gamma_1 \langle \boldsymbol{w}\boldsymbol{w} \rangle : \nabla \boldsymbol{u} + \gamma_2 \langle c w_3 \rangle - \gamma_3 \epsilon \right] \tag{27}$$

where $\gamma_1$, $\gamma_2$ and $\gamma_3$ are appropriate constants of order 1 (e.g., Lumley, 1978; Rodi, 1987).

Most authors, however, insist on the constraining hypotheses needed to derive such simple expressions and on the empirical character of eq. 27 which makes the $\epsilon$-equation the weak link in any $k$–$\epsilon$ model.

Attempts to replace eq. 25 by an equation for $l_m$ or a combination of $l_m$ and $\epsilon$ have brought no significant improvement (Blumberg and Mellor, 1985; Rodi, 1987).

Recent developments in three-dimensional modelling seem to suggest that, in the case of shallow shelf seas where a fairly good repre-

sentation of $l_m$ can be induced from long series of observations, more reliable results can be obtained by leaving out the $\epsilon$-equation and closing the model at the $k$-equation, complemented by eqs. 20 and 21 and the appropriate empirical equation for $l_m$.

The eddy diffusivities $\tilde{\nu}^a$, $\tilde{\nu}^k$, $\tilde{\nu}^\epsilon$ are usually referred to the eddy viscosity $\tilde{\nu}$ by equations of the form

$$\tilde{\nu}^i = \tilde{\nu}\psi^i \quad i = a,\ k,\ \epsilon \tag{28}$$

where the $\psi^i$'s are non-dimensional functions.

The determination of these functions in adequate parametric form is part of the calibration of the model.

## 2 APPLICATION OF $k-\epsilon$ MODELS TO MARINE GEOHYDRODYNAMICS

Ensemble averages, although extremely useful for the presentation of the basic concepts of turbulence, are not applicable in practice and they are usually replaced, in geophysical fluid dynamics, by time averages.

The conditions for a time average to provide a good approximation of an ensemble average have been discussed by many authors. One essential requirement is that the period of time over which the average is made corresponds to a valley in the energy spectrum of motions, separating a "mean flow", at larger scales, from "fluctuations" at smaller scales.

If one refers to Table I, one can see that time averaging can be a much richer—even if approximate—tool than ensemble averaging.

One can indeed select, by time averaging, any specific spectral window of interest and write appropriately tuned equations, smoothing out smaller scale processes in much the same way as one does for turbulence, keeping only the overall "diffusion" effect of sub-grid scale fluctuations.

Marine forecasting is essentially concerned with the so-called "weather of the sea" which includes processes from the mesoscale tides and storm surges to synopticscale fronts and ocean rossbies and quasi-steady seasonalscale currents generally referred to as the "general circulation".

Table I shows that even models of mesoscale motions require an extension of the concept of turbulence described in the previous section. Sub-window scale processes include indeed—in addition to microscale three-dimensional fluctuations quite assimilable to turbulence as described above—mesialscale processes affected by the stratification.

In the ocean, the stratification inhibits vertical motions and constrains turbulent patches to pancake clusters referred to as "blinies". Epidermic (Kelvin-Helmoltz) instabilities of the blinies' interfaces produce breaking waves and new patches of turbulence, evolving into smaller blinies. These, in turn, are the seat of epidermic instabilities and the source of smaller blinies.

This mechanism and the breaking of internal waves and other non-linear processes result in a down-scale cascade of energy reminiscent of the turbulent cascade (e.g., Nihoul, 1980). The associated vertical mixing, however, is affected by the stratification and by the intermittency of bliny turbulence.

In sufficiently shallow shelf seas, the surface and bottom mixed layers entrain, in 3D boundary layer turbulence, increasing portions of the intermediate layers of intermittent turbulence.

The associated vertical mixing may produce fairly homogeneous water columns—justifying 2D depth-averaged models—but, if the boundary conditions are right, a sharp pycnocline may be maintained between the two layers and the local effect of the stratification on the turbulent vertical diffusivities must be taken into account.

This effect is generally measured by the "Richardson number":

$$Ri = \frac{\left|\dfrac{\partial a}{\partial x_3}\right|}{\nabla \boldsymbol{u} : \nabla \boldsymbol{u}} \tag{29}$$

or the "flux Richardson number":

$$R_f = \frac{|\langle w_3 c\rangle|}{\langle -\boldsymbol{w}\boldsymbol{w}\rangle : \nabla \boldsymbol{u}} \tag{30}$$

In eqs. 16, 17, 24 and 26, scalar eddy diffusivities have been introduced. This can only be valid if horizontal and vertical diffusions have the same efficiency and, obviously, is not strictly applicable to stably stratified fluids where vertical mixing is inhibited.

However, if the horizontal and vertical eddy diffusivities associated with mesialscale–microscale fluctuations, affected by the stratification, are not the same, one may argue that they remain of comparable orders of magnitude.

In that case, the characteristic length scales of horizontal variations being considerably larger than the vertical length scales, the horizontal divergence of a turbulent flux is much smaller than the $x_3$-derivative of its vertical component. In other words, horizontal diffusion may be neglected as compared to vertical diffusion. This does not imply that there is no horizontal diffusion in nature. It simply means that, at this stage, the main part is still concealed in the advection term which contains irregular and variable horizontal currents responsible for a form of horizontal "pseudo turbulence" (e.g., Nihoul, 1975; Monin and Ozmidov, 1985).

The discrepancy between horizontal and vertical length scales, however, imposes, in most cases, numerical grids with much larger horizontal meshes. The discretization of the equations is then equivalent to performing a second (horizontal space) average and nonlinear interactions of sub-grid scale fluctuations are responsible for an additional horizontal diffusion which it is convenient to introduce explicitly in the mathematical evolution equations, anticipating the subsequent discretization.

The sub-grid scale horizontal diffusivities can be related to the mesh size and to the turbulent energy dissipation rate in the associated range of scales using an extension of Kolmogorov's theory developed by Ozmidov (e.g., Nihoul, 1975; Monin and Ozmidov, 1985). In many cases, they can be taken as constants.

The vertical eddy diffusivities, on the other hand, are functions of the stratification and the same is true for the mixing length and for the ratio $\psi^a$ of the diffusivities of buoyancy and momentum.

This is easily understood.

In a stratified fluid, work has to be done to raise an isolated blob of fluid above its equilibrium level. In zero shear (i.e., $Ri = \infty$), the blob of fluid will fall back to its equilibrium level at a rate determined by the Brunt-Väisälä frequency $|\partial a/\partial x_3|^{1/2}$. As the shear increases (i.e., as $Ri$ decreases), the tendency for a displaced parcel of fluid to return to its equilibrium level will decrease, but there will still be a buoyancy force acting on it to make it return. As the blob of fluid is temporarily displaced from its equilibrium position it will exchange its properties with the surrounding fluid at the new level. In the case of temperature, salinity, buoyancy and other scalar properties of the fluid, complete exchange can only be effected by small-scale turbulent mixing and ultimately by molecular action. This takes a considerable time and usually the parcel of fluid will be dragged back to its equilibrium level before it can exchange more than a tiny fraction of its heat, salt, buoyancy with its new and dissimilar surroundings during its temporary residence there.

For momentum, however, the situation is different. The blob of displaced fluid has a different horizontal velocity than its new surroundings (i.e., there is a shear), and there is a drag on it. This is a bulk force which requires no molecular mixing-in: the momentum is transferred immediately by pressure.

Thus momentum exchange is likely to retain its efficiency at high Richardson number, even though the buoyancy transfer is reduced as the stratification increases. One should thus expect:

$$\psi^a = \psi^a(Ri \text{ or } R_f) < 1 \tag{31}$$

The functions $\psi^k$ and $\psi^\epsilon$, on the other hand, are generally assumed constant and of order 1.

The determination of $\tilde{\nu}$, $\psi^a$ and $l_m$ as functions of the Richardson number, in the

scope of any particular model, is based both on the general understanding of the processes involved and on the appreciation of the specific conditions of the problem. The formulation of appropriate empirical formulas, after critical review of the literature and exploitation of the data base, is part of the "calibration" of the model.

If the parameterization is made with care and the stratification is correctly taken into account, it is then commonly accepted that mesialscale and microscale processes—the sub-window scale processes of mesoscale models—constitute a sufficiently varied ensemble of rapidly changing and chaotic motions to be described by a form of turbulence theory and that, at least for shallow shelf seas, $k$–$\epsilon$ models (modified for stratification constraints) are applicable to short-range marine weather forecasting (e.g., Nihoul and Djenidi, 1987).

Whether this is equally true for long-range (general circulation) marine weather forecasts is a question which deserves more discussion and which will be addressed in the next section.

## 3 APPLICATION OF $k$–$\epsilon$ MODELS TO THE DETERMINATION OF THE GENERAL CIRCULATION

Although mesoscale processes such as storm surges have an obvious influence on the marine system and strongly affect observations, the final interpretation of data and the description of ecological processes, and the corresponding physical constraints, require a sound understanding of the long-term displacement of water masses, the cumulated deposition of sediments, the persistence of upwellings and the progressive deployment of their plumes' instabilities. What is needed is a comprehensive synthetic picture of synoptic- and macroscale processes which characterize the horizontal and vertical transports and diffusions at, say, monthly or seasonal scales, that one often refers to as the "general circulation" of the sea.

To model the general circulation, it is tempting to consider long time averages (several weeks) and, identifying the highlighted macroscale flow with the "mean flow" of $k$–$\epsilon$ models, treat all smaller scale motions as "fluctuations", following the same reasoning as before.

It is doubtful, however, that the parameterization schemes discussed in section 1 can be applied to sub-window scale fluctuations which now include mesoscale processes such as tides and wind-induced currents.

These processes—even if they often appear suitably chaotic thanks to wind variations and long waves' multiple reflections and non-linear interactions—have incommensurable horizontal and vertical characteristics with several orders of magnitude differences in length scales and energy.

The $k$–$\epsilon$ closure is based on arguments inspired by three-dimensional isotropic turbulence. These arguments may presumably be adapted—at least in the case of shelf seas—to mesialscale fluctuations, as discussed in section 2, but their extension to highly anisotropic mesoscale fluctuations would be foolhardy.

If one defines the general circulation as the average over a time $T$ of several weeks (i.e., much larger than the characteristic time of tides, passing storms and other mesoscale processes), one can write, averaging eqs. 9, 10, 11, 22 and 25:

$$\nabla \cdot \boldsymbol{u}_0 = 0 \tag{32}$$

$$\frac{\partial \boldsymbol{u}_0}{\partial t} + \nabla \cdot (\boldsymbol{u}_0 \boldsymbol{u}_0) + 2\boldsymbol{\Omega} \wedge \boldsymbol{u}_0 = -\nabla q_0 + \boldsymbol{a}_0 - \nabla \cdot (\boldsymbol{u}_1 \boldsymbol{u}_1)_0 - \nabla \cdot \tilde{\boldsymbol{\Phi}}_0^u \tag{33}$$

$$\frac{\partial a_0}{\partial t} + \nabla \cdot (\boldsymbol{u}_0 a_0) = -\nabla \cdot (\boldsymbol{u}_1 a_1)_0 - \nabla \cdot \tilde{\phi}_0^a \tag{34}$$

$$\frac{\partial k_0}{\partial t} + \nabla \cdot (\boldsymbol{u}_0 k_0) = Q_0^k - \nabla \cdot (\boldsymbol{u}_1 k_1)_0 - \nabla \cdot \tilde{\phi}_0^k \tag{35}$$

$$\frac{\partial \epsilon_0}{\partial t} + \nabla \cdot (\boldsymbol{u}_0 \epsilon_0)$$

$$= Q_0^\epsilon - \nabla \cdot (\boldsymbol{u}_1 \epsilon_1)_0 - \nabla \cdot \tilde{\phi}_0^\epsilon \qquad (36)$$

In these equations the subscript "0" denotes the general circulation while the subscript "1" refers to superimposed mesoscale motions.

The time of integration $T$ is, by choice, large compared to the characteristic time of the latter and small compared to the characteristic time of the former. Thus, $y$ standing for any state variable,

$$\frac{1}{T}\int_t^{t+T} \frac{\partial y}{\partial t}\, \mathrm{d}t$$

$$= \frac{1}{T}\int_t^{t+T}\left(\frac{\partial y_0}{\partial t} + \frac{\partial y_1}{\partial t}\right) \mathrm{d}t$$

$$\sim \frac{1}{T}\int_t^{t+T} \frac{\partial y_0}{\partial t}\, \mathrm{d}t = \frac{y_0(t+T) - y_0(t)}{T}$$

$$\sim \frac{\partial y_0}{\partial t}$$

The time derivatives in eqs. 32–36 represent, however, small contributions which can be neglected in the mathematical model. They are retained here for the sake of completeness and to allow for numerical methods of resolution which determine the steady-state as the asymptote of a non-steady evolution from given initial conditions under stationary forcings and boundary conditions.

One emphasizes that $k_0$ and $\epsilon_0$ are respectively the averages over $T$ of the kinetic energy and energy dissipation rate associated with mesialscale and microscale processes. In particular, $k_0$ is not the kinetic energy of all sub-$T$ scale processes as one would have in a blunt application of the $k$–$\epsilon$ closure.

The mean turbulent energy production rate $Q_0^k$ is given by:

$$Q_0^k = -\langle \boldsymbol{ww} \rangle_0 : \nabla \boldsymbol{u}_0 - [\langle \boldsymbol{ww} \rangle : \nabla \boldsymbol{u}_1]_0 + \langle cw_3 \rangle_0 - \epsilon_0 \qquad (37)$$

The first term and the last two terms in the right-hand side involve simple macroscale quantities. The second term is more complicated and will be discussed in more detail in the next section.

The macroscale average of $Q^\epsilon$ is, comparatively, a desperate case. Considering the nonlinearities of eq. 27, it is far from obvious how a simple expression involving well-identified macroscale mean values or fluxes could ever be conceived.

This casts doubts on the possibility of any realistic use of the $\epsilon$-equation at general circulation level and recommends to fall back on simple closure schemes where the $k$-equation is complemented by some appropriate algebraic semi-empirical relationship between $\epsilon$, $k$, $l_m$ and $R_f$ supplanting eq. 36. (The so-called "mixing length approximation".)

The turbulent kinetic energy $k$, the turbulent energy dissipation rate $\epsilon$ and the turbulent fluxes $\tilde{\phi}$ are defining features of the average contribution of small scale (microscale to mesialscale) fluctuations. Averaging over a time $T$ much larger than the characteristic times of these fluctuations is merely taking the mean of a long sequence of almost identical statistical samples and does little except eroding time variations to form quasi-steady macroscale averages $k_0$, $\epsilon_0$, $\tilde{\phi}_0, \ldots$

It is conceivable then that the same structural relationships and scalings persist between these quantities and one may argue that the concepts of eddy diffusivities and mixing length and the parametric expressions between them (eqs. 20 and 21, for instance) are transposable to models of the general circulation.

In this context, the appropriate measure of the stratification is the macroscale flux Richardson number:

$$R_f^0 = \frac{|\langle cw_3 \rangle|_0}{[\langle -\boldsymbol{ww} \rangle : \nabla \boldsymbol{u}]_0} \qquad (38)$$

where the denominator is the total production rate, i.e. the sum of the first two terms in the right-hand side of eq. 27.

The second term represents the average contribution of mesoscale processes and must be collated with the mesoscale "Reynolds" stresses $\langle \boldsymbol{u}_1 \boldsymbol{u}_1 \rangle_0$ and fluxes $\langle \boldsymbol{u}_1 a_1 \rangle_0$, $\langle \boldsymbol{u}_1 k_1 \rangle_0$,

... and similar terms in the formulation of the boundary conditions.

They will be discussed in the next sections.

## 4 MESOSCALE "REYNOLDS" STRESSES AND FLUXES

In shelf seas, mesoscale and turbulent fluxes play a quite different role in the macroscale dynamics.

Mesoscale processes are characterized by energetic horizontal motions and large horizontal length scales and, by the continuity equation, weak vertical motions and vertical length scales not exceeding the depth. Small scale turbulence has comparable length scales and velocity scales in the horizontal and in the vertical.

If $L_1$ and $u_1$ denote typical horizontal length and velocity scales for mesoscale motions in a shelf sea, the associated vertical velocity scales for mesoscale and turbulent flows are given respectively by (e.g., Nihoul, 1975, 1977a, b, 1982):

$$u_v \sim \frac{u_1 H}{L_1} \text{ (mesoscale)}$$

(where $H$ is the depth)

$$u_* \sim D^{\frac{1}{2}} u_1 \text{ (turbulent)}$$

(where $D$ is the drag coefficient). Taking $H \sim 50$ m, $L_1 \sim 10^5$ m, $D \sim 3 \cdot 10^{-3}$, one finds:

$$\frac{u_v}{u_*} \sim \frac{H}{L_1 D^{\frac{1}{2}}} \sim 10^{-2}$$

Thus, the vertical mesoscale advection is small and the vertical mixing associated with its variability may be neglected as compared with typical turbulent vertical mixing. The mesoscale fluxes reduce to their horizontal components.

To assess the importance of these fluxes, it is instructing to consider two asymptotic cases: (1) a well-mixed shelf sea like the North Sea in the winter where tides are dominant—imposing recurrent structures on the mesoscale flow fields—together with intense storm surges and where mesoscale velocities can be one or two orders of magnitude larger than residual velocities; (2) a stratified shelf sea like the Northern Bering Sea in the summer where tidal motions are relatively small, wind-induced currents comparatively versatile and where mesoscale velocities are comparable with typical macroscale current speeds.

In the first case, assuming $u_1 \sim 1$ ms$^{-1}$, $u_0 \sim 10^{-1}$ m s$^{-1}$ and taking into account that the relative coherence imposed by the dominant tides maintains the average $(\boldsymbol{u}_1\boldsymbol{u}_1)_0$ a substantial fraction of $\boldsymbol{u}_1\boldsymbol{u}_1$, one can write conservative estimates of

$\nabla \cdot (\boldsymbol{u}_0\boldsymbol{u}_0)$, $\nabla \cdot (\boldsymbol{u}_1\boldsymbol{u}_1)_0$, $2\boldsymbol{\Omega} \wedge \boldsymbol{u}_0$ as:

$$\nabla \cdot (\boldsymbol{u}_0\boldsymbol{u}_0) \sim 10^{-7}$$

$$\nabla \cdot (\boldsymbol{u}_1\boldsymbol{u}_1)_0 \sim 10^{-5}$$

$$2\boldsymbol{\Omega} \wedge \boldsymbol{u}_0 \sim 10^{-5}$$

The mesoscale Reynolds stress is thus an essential forcing of the general circulation (as important as the Coriolis effect) and it must be taken into account as accurately as possible.

In the second case, assuming $u_1 \sim u_0 \sim 3 \cdot 10^{-1}$ ms$^{-1}$ and allowing for one order of magnitude difference between $\boldsymbol{u}_1\boldsymbol{u}_1$ and $(\boldsymbol{u}_1\boldsymbol{u}_1)_0$ in the absence of dominant cohesive tidal motions, one finds:

$$\nabla \cdot (\boldsymbol{u}_0\boldsymbol{u}_0) \sim 10^{-6}$$

$$\nabla \cdot (\boldsymbol{u}_1\boldsymbol{u}_1)_0 \sim 10^{-7}$$

$$2\boldsymbol{\Omega} \wedge \boldsymbol{u}_0 \sim 3 \cdot 10^{-5}$$

The mesoscale flux of momentum is thus a relatively small effect and one may argue that it can be parameterized as simple horizontal diffusion. This effect may then be combined with the horizontal sub-grid scale diffusion mentioned in section 2 and associated with the horizontal resolution of the numerical grid.

A similar approximation may presumably be made for the mesoscale fluxes of buoyancy and turbulent kinetic energy (the comparison is made here between mesoscale diffusion and advection by the general circulation).

To understand the implications of this approximation, it is illuminating to discuss

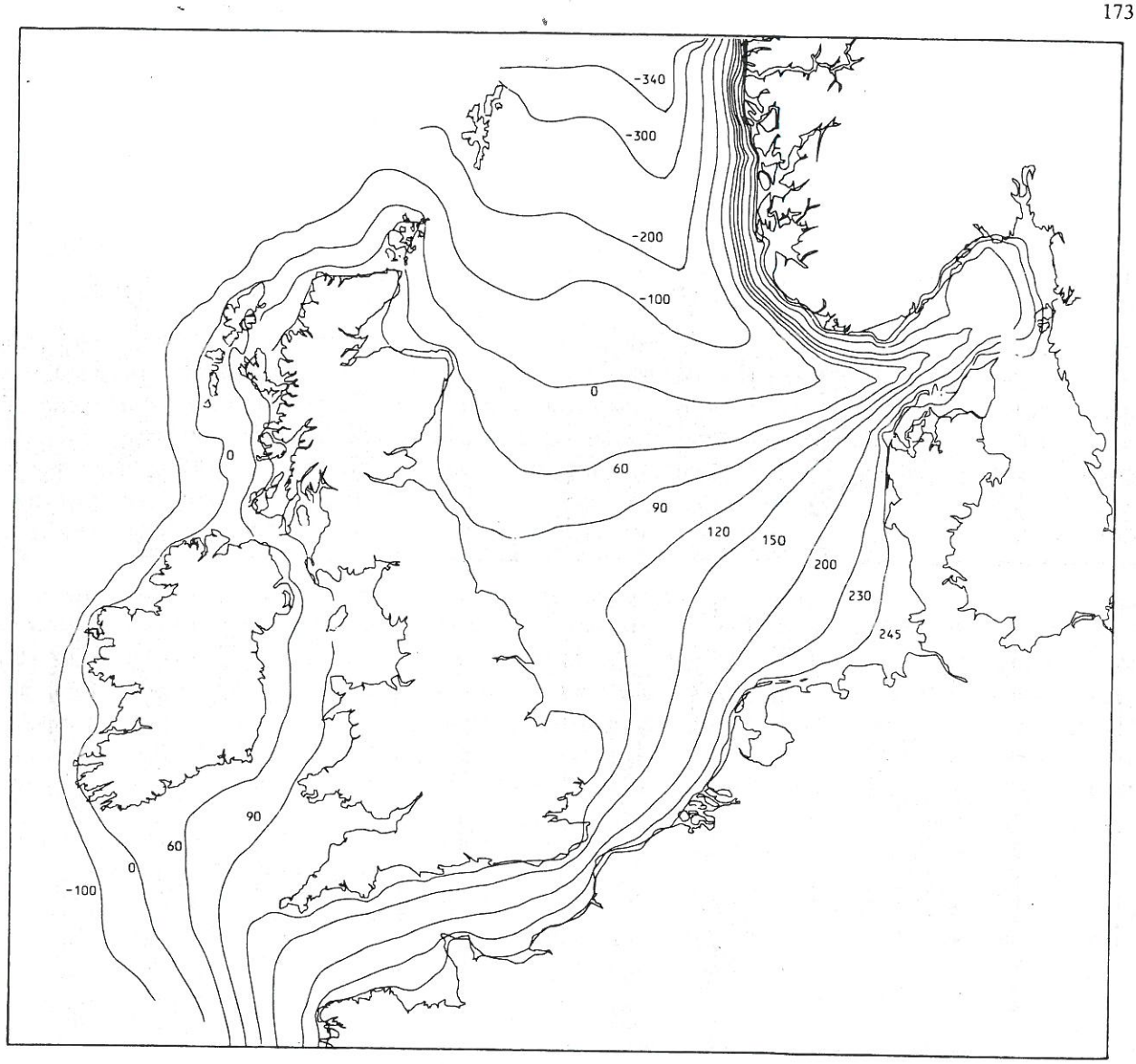


Fig. 1. Streamlines of the depth-integrated general circulation (graduated in $10^3$ $m^3s^{-1}$) on the Northwestern European Continental Shelf when the residual wind stress is neglected and the mesoscale Reynolds stresses are not taken into account.

briefly the role of the mesoscale Reynolds stresses in shallow shelf seas satisfying the conditions of case 1. In this case, the mesoscale Reynolds stress tensor is an essential forcing and should be calculated explicitly.

The same would be true, of course, of the corresponding fluxes of buoyancy and turbulent kinetic energy.

Fortunately, the turbulence generated by the intense mesoscale currents destroys the stratification. Then much simpler models (2D, 2D + 1D, ...) may be used, leaving aside completely buoyancy and turbulent kinetic energy (e.g., Nihoul, 1975, 1977b; Nihoul and Djenidi, 1987).

On the other hand, the predominance of the energetic mesoscale motions allows their prior determination, independently of the weak residual component. The preliminary forecasts of a few typical mesoscale situations and the collation of the model's results with all available observations provide the neces-

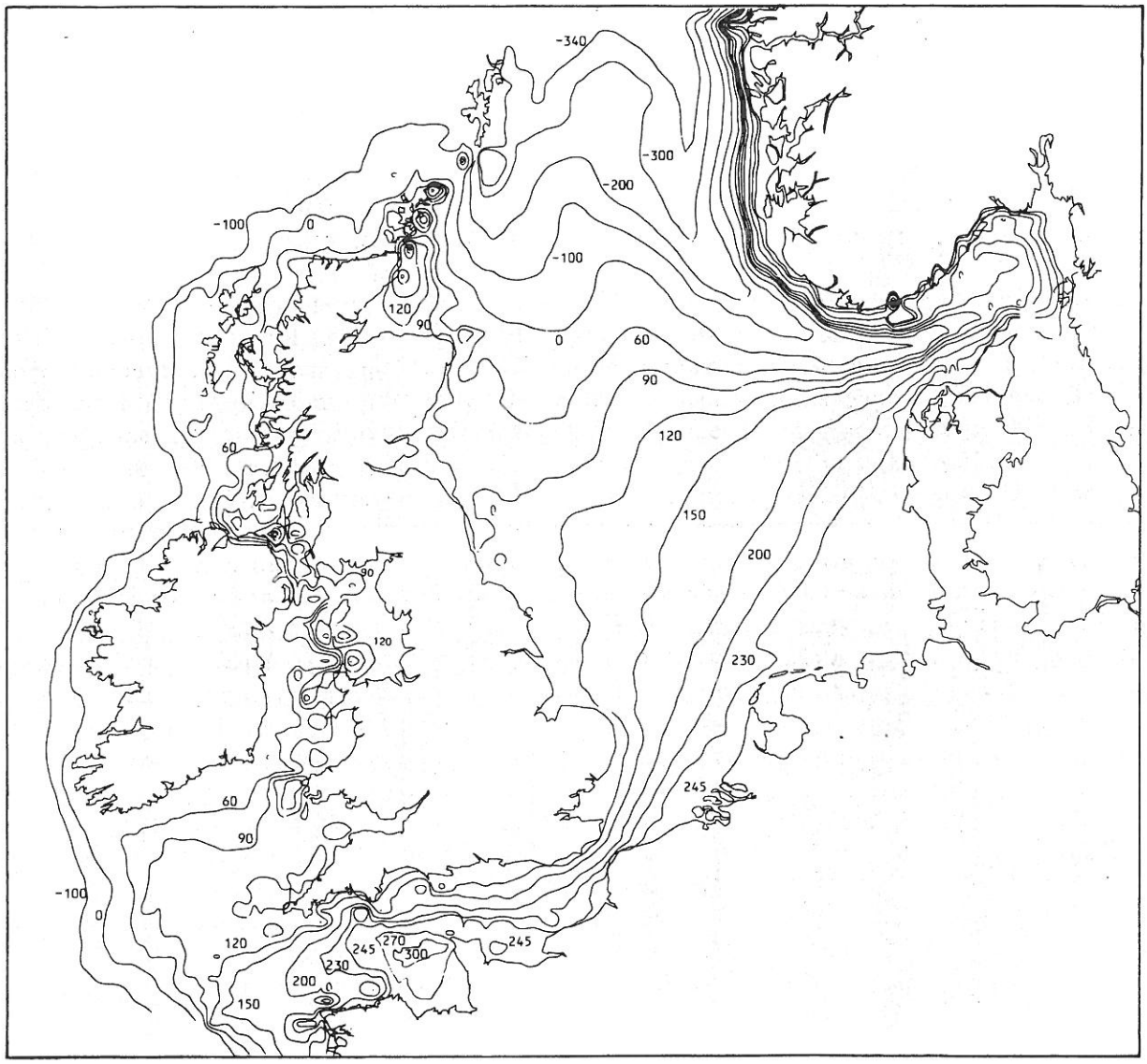


Fig. 2. Streamlines of the depth-integrated general circulation (graduated in $10^3$ $m^3s^{-1}$) on the Northwestern European Continental Shelf when the residual wind stress is neglected and the mesoscale Reynolds stresses are taken into account.

sary data base to compute explicitly, with a sufficient degree of accuracy, the mesoscale Reynolds stress tensor and apply it, as a given forcing, in the equations for the general circulation (Nihoul, 1975, 1977a, b, 1982; Djenidi, 1987; Nihoul and Djenidi, 1987).

In many cases, this additional forcing is found responsible for the appearance, in the general circulation flow pattern, of local secondary flows having the form of gyres, marked by closed stream-lines. These gyres, although disrupted and moved along by tidal currents, contribute nevertheless to increase the residence time of water masses in the area and may significantly affect the transfer of marine contaminants (e.g. Nihoul, 1982).

This situation is particularly well illustrated by the results of a simulation of the general circulation and long-term transports of pollutants on the Northwestern European Continental Shelf (Djenidi, 1987).

Fig. 1 shows the streamlines of the

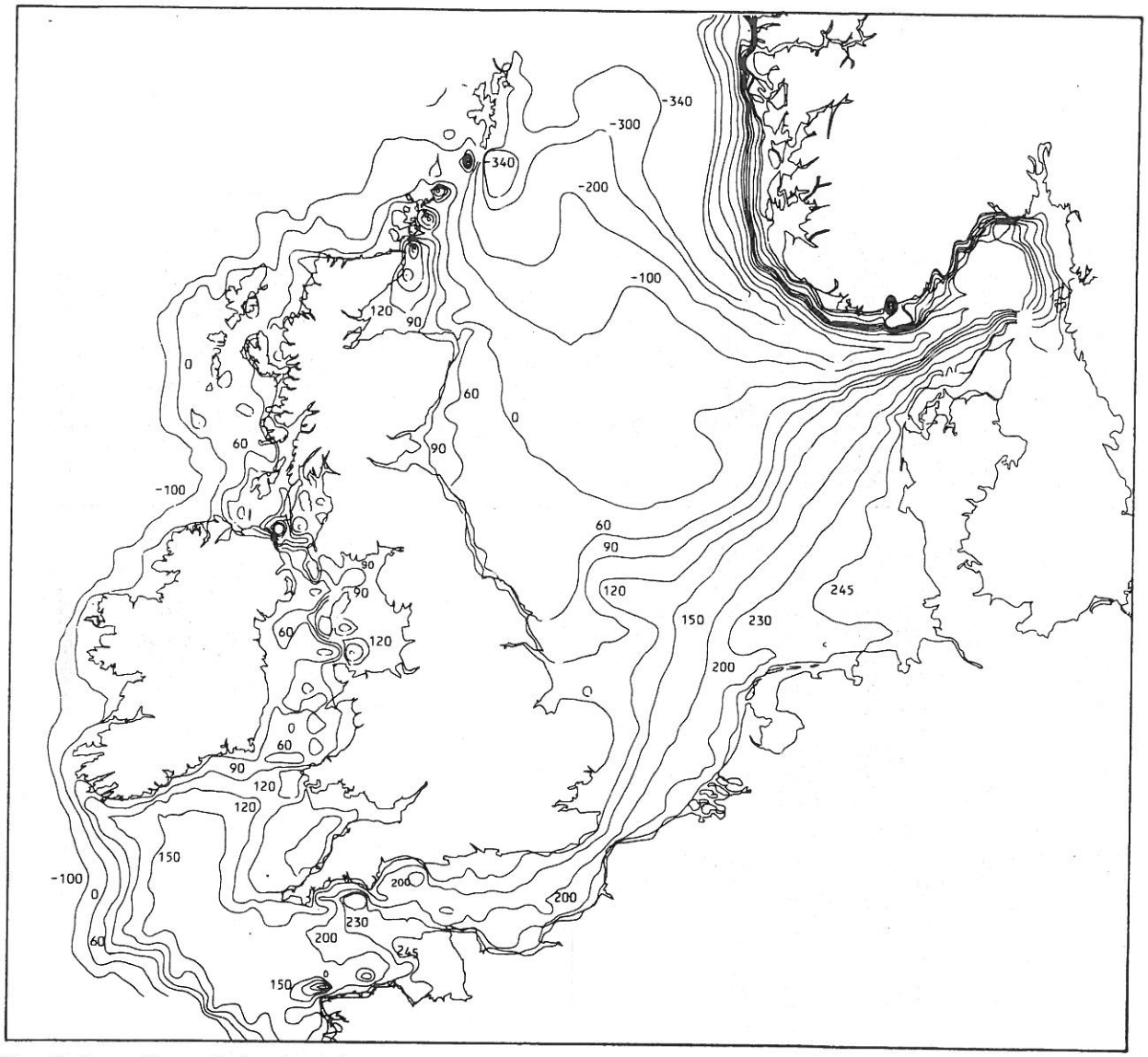


Fig. 3. Streamlines of the depth-integrated general circulation (graduated in $10^3$ $m^3s^{-1}$) on the Northwestern European Continental Shelf with mesoscale Reynolds stress forcing and real wind forcing (typical winter situation).

depth-integrated general circulation when the residual wind stress is neglected and the mesoscale Reynolds stresses are not taken into account. The flow is forced in this case by the inflows and the outflows at the open-sea boundaries only. Fig. 2 shows the same result when the mesoscale Reynolds stress forcing is applied but no residual wind forcing. Figs. 3 and 4 show the general circulation when both forcings are included, for typical winter and summer situations.

The tendency of the mesoscale Reynolds stresses to generate secondary gyres is manifest.

In situations pertaining to case 2, such gyres are not excluded but it is reasonable to expect the impact of the comparatively less energetic and more chaotic mesoscale motions to be less important and eventual secondary flows to be weaker and negligible. In these conditions, the approximation of the effect of the mesoscale fluxes by simple hori-

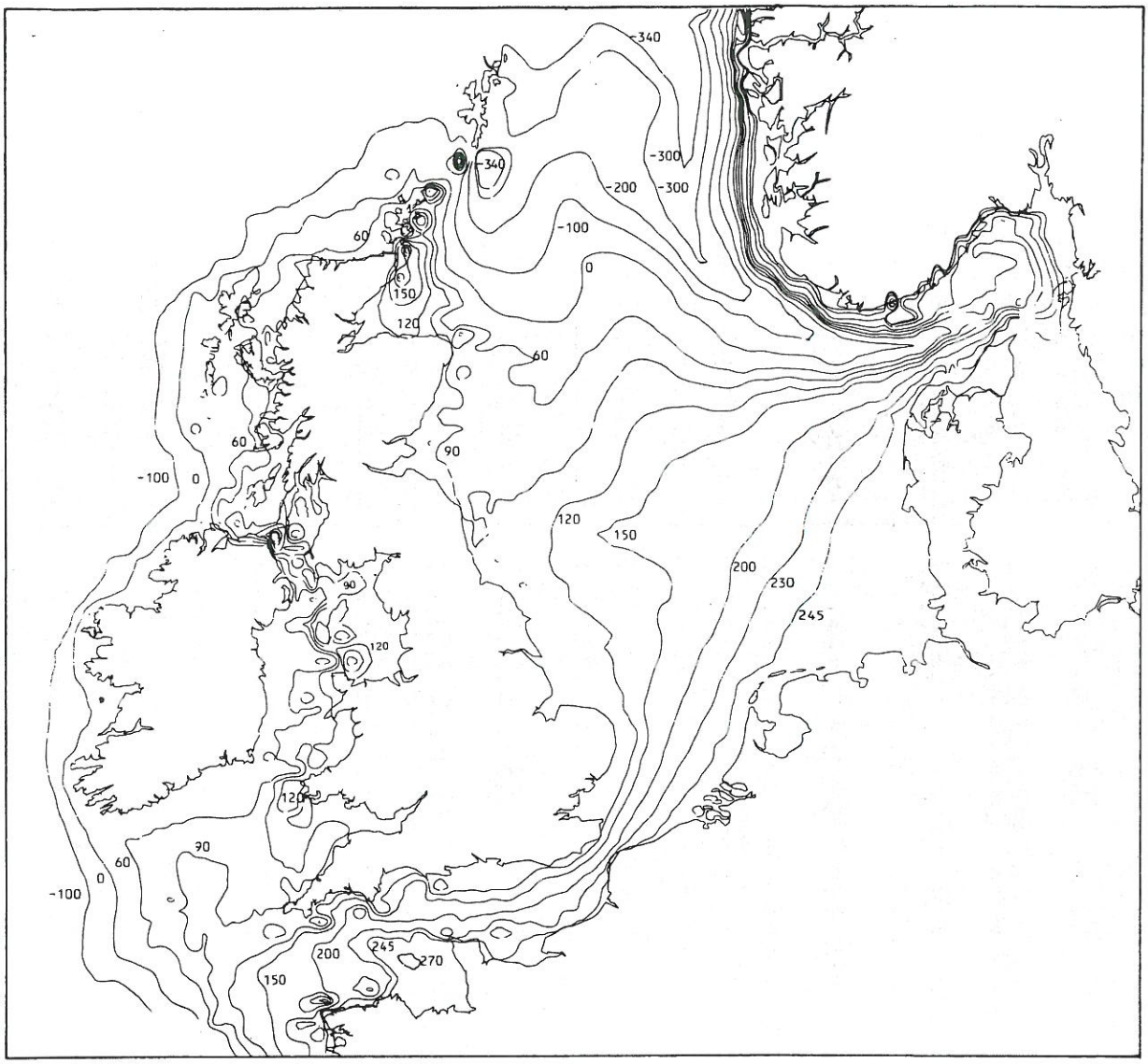


Fig. 4. Streamlines of the depth-integrated general circulation (graduated in $10^3$ $m^3$ $s^{-1}$) on the Northwestern European Continental Shelf with mesoscale Reynolds stress forcing and real wind forcing (typical summer situation).

zontal diffusion terms, which do not allow secondary flow structures, is probably acceptable.

## 5 MESOSCALE AIR–SEA INTERACTIONS AND TURBULENT ENERGY PRODUCTION

The boundary conditions compatible with eqs. 32–35 must bear on the same mean variables or fluxes. In particular, at the air–sea interface, the mean turbulent fluxes of momentum, buoyancy, turbulent energy,... must be—allowing for surface sources and sinks—continuous.

Because turbulent fluxes are non-linear functions of state variables' differences between air and water (e.g., Nihoul, 1975), the mean fluxes cannot be related to mean values of atmospheric and marine quantities. The main contribution is the macroscale average of products of mesoscale fluctuations and this must be evaluated separately from statistics of wind fields, air temperatures and humidi-

ties, cloud covers, rainfalls, sea surface temperatures ... over the mesoscale range. The part directly played by macroscale processes is comparatively negligible.

Thus, at the level of the general circulation, air–sea exchanges act as predetermined boundary constraints, independent of the computed macroscale state of the sea.

This incidently provides an argument for using a buoyancy equation instead of two equations for temperature and salinity and an empirical relationship relating their values to buoyancy.

The objections to a single buoyancy equation have always been that: (1) molecular fluxes of heat and salt do not correctly combine into a single flux of buoyancy because of definite differences in molecular diffusivities; and (2) boundary conditions at the air–sea interface are expressed in terms of heat and salt fluxes which require the explicit determination of marine state variables such as the sea-surface temperature.

The first objection may be discarded because molecular diffusion is, in any case, completely negligible as compared with turbulent diffusion.

The second objection does not hold for general circulation models since boundary fluxes of buoyancy are now calculated from macroscale averages of heat fluxes and salt fluxes using climatological data independent of the model's predictions.

Another mesoscale effect which is related to air–sea interactions is the contribution of mesoscale transfers of momentum to the production of turbulent kinetic energy in the upper layer of the sea (the second term in the right-hand side of eq. 37).

In the case of well-mixed shelf seas where simple (depth-integrated) models can be used and the turbulent kinetic energy equation may be dispensed with, the parameterization of the mesoscale energy production rate is not needed but it may play an important role in stratified systems requiring fully three-dimensional models.

An explicit preliminary calculation of this contribution—as for the mesoscale Reynolds stresses in well-mixed tidal seas—does not seem possible in this case but numerous process models of the ocean's mixed layer are available, providing valuable information on the magnitude and depth penetration of transient wind mixing.

As shown by Kitaigorodskii (1979), energy production is maximum in the subsurface layer and decreases rapidly with depth. The total rate of production (integrated over depth) is of the order of $\beta\tau_w^{3/2}$ where $\tau_w$ is the wind stress (per unit mass of sea water) and $\beta \sim 10$.

The scaling factor for the second term in the right-hand side of eq. 37 is thus $\beta[\tau_w^{3/2}]_0$ and it may be calculated following the same routine as for the boundary fluxes at the air–sea interface.

This scaling factor must then be multiplied by an appropriate profile function which distributes the energy production rate over depth. The determination of the profile function must take into account observations, conceptual results of sideways process models but also requirements of the numerical method and resolution. (The results are not prohibitively sensitive to the exact form of the profile function as long as the physics is correctly represented.) The effect of the stratification (depth of the pycnocline ...) may be included by allowing the profile function to depend on the Richardson number (Deleersnijder and Nihoul, 1988).

## 6 THE GHER 3D MODEL FOR THE STUDY OF THE GENERAL CIRCULATION

The three-dimensional model developed at the GeoHydrodynamics and Environment Research laboratory (GHER) of the University of Liège is based on the equations and parametric formulas discussed in the previous sections. The additional quasi-hydrostatic approximation is made and vertical velocities are neglected in the horizontal components of the Coriolis acceleration, as it is customary in

the study of large scale motions (e.g. Nihoul, 1975, 1977a).

In the version of the model appropriate to the study of the general circulation in shelf seas, the state variables are the three components of the velocity vector, the pressure (or $q$), the buoyancy and the turbulent kinetic energy. The evolution equations are derived from eqs. 32, 33, 34 and 35.

In the frame of the quasi-hydrostatic approximation, the vertical component of eq. 33 reduces to a simple balance between buoyancy and vertical gradient of $q$.

The mesoscale horizontal Reynolds stresses and fluxes of buoyancy and energy are taken into account in global horizontal diffusion terms which also include sub-grid scale diffusion and the small contribution of small scale turbulence. The horizontal diffusivities are assumed constant (but their values may be functions of the size of the mesh).

Vertical turbulent fluxes are assumed proportional to the vertical gradients of the mean fields' characteristics and the diffusivity coefficients are related to the mixing length and the turbulent kinetic energy through eqs. 20, 21 and 28. The mixing length is a function of depth and of the flux Richardson number.

The mesoscale energy production rate is written:

$$\pi = \left[\langle -\boldsymbol{ww}\rangle : \nabla \boldsymbol{u}_1\right]_0 \sim \beta\left[\tau_w^{3/2}\right]_0 \tag{39}$$

where $\beta$ is also a function of the depth and the flux Richardson number.

The boundary conditions are calculated as described in section 5.

Dropping the subscript "0" for simplicity one may then write the basic equations as follows:

$$\frac{\partial u_1}{\partial x_1} + \frac{\partial u_2}{\partial x_2} + \frac{\partial u_3}{\partial x_3} = 0 \tag{40}$$

$$\frac{\partial u_1}{\partial t} + \nabla \cdot (\boldsymbol{u}u_1) - fu_2 = -\frac{\partial q}{\partial x_1} + \tilde{\mu}\Delta u_1 + \frac{\partial}{\partial x_3}\left(\tilde{\nu}\frac{\partial u_1}{\partial x_3}\right) \tag{41}$$

$$\frac{\partial u_2}{\partial t} + \nabla \cdot (\boldsymbol{u}u_2) + fu_1 = -\frac{\partial q}{\partial x_2} + \tilde{\mu}\Delta u_2 + \frac{\partial}{\partial x_3}\left(\tilde{\nu}\frac{\partial u_2}{\partial x_3}\right) \tag{42}$$

$$\frac{\partial q}{\partial x_3} = a \tag{43}$$

$$\frac{\partial a}{\partial t} + \nabla \cdot (\boldsymbol{u}a) = \tilde{\mu}^a \Delta a + \frac{\partial}{\partial x_3}\left(\tilde{\nu}^a \frac{\partial a}{\partial x_3}\right) \tag{44}$$

$$\frac{\partial k}{\partial t} + \nabla \cdot (\boldsymbol{u}k) = Q^k + \tilde{\mu}^k \Delta k + \frac{\partial}{\partial x_3}\left(\tilde{\nu}^k \frac{\partial k}{\partial x_3}\right) \tag{45}$$

where $f$ is twice the vertical component of the earth's rotation vector, $\tilde{\mu}$ is the horizontal (mesoscale + turbulent) viscosity, $\tilde{\nu}$ the vertical turbulent viscosity, $\tilde{\mu}^a$ and $\tilde{\mu}^k$ respectively the horizontal (mesoscale + turbulent) diffusivities of buoyancy and turbulent kinetic energy, $\tilde{\nu}^a$ and $\tilde{\nu}^k$ respectively the vertical turbulent diffusivities of buoyancy and energy and where:

$$Q^k = \tilde{\nu}\frac{\partial \boldsymbol{u}}{\partial x_3} \cdot \frac{\partial \boldsymbol{u}}{\partial x_3} + \pi - \tilde{\nu}^a \frac{\partial a}{\partial x_3} - \epsilon \tag{46}$$

(with $\pi$ given by eq. 39)

$$\Delta = \frac{\partial^2}{\partial x_1^2} + \frac{\partial^2}{\partial x_2^2} \tag{47}$$

It is assumed that:

$$\tilde{\mu}^a = \alpha^a \tilde{\mu}; \quad \tilde{\mu}^k = \alpha^k \tilde{\mu} \tag{48); (49}$$

$$\tilde{\nu}^a = \psi^a \tilde{\nu}; \quad \tilde{\nu}^k = \psi^k \tilde{\nu} \tag{50); (51}$$

$$\tilde{\nu} = 0.5\tilde{\alpha}^{\frac{1}{2}} l_m k^{\frac{1}{2}} \tag{52}$$

$$\epsilon = \tilde{\alpha} k^2 (16\tilde{\nu})^{-1} \tag{53}$$

where $\tilde{\alpha}$, $\alpha^a$, $\alpha^k$ and $\psi^k$ are taken as constants of order 1 and $\psi^a$ is a function of the flux Richardson number:

$$R_f = \frac{\tilde{\nu}^a \left|\frac{\partial a}{\partial x_3}\right|}{\tilde{\nu}\left\|\frac{\partial \boldsymbol{u}}{\partial x_3}\right\|^2 + \pi} \tag{54}$$

The model is closed by providing suitable empirical expressions for $l_m(x_3, R_f)$, $\beta(x_3, R_f)$ and $\psi^a(x_3, R_f)$, using (historical or specific) data and theoretical results and taking into account the requirements of the numerical scheme (e.g. Nihoul, 1975; Nihoul and Djenidi, 1987; Deleersnijder and Nihoul, 1988).

## 7 APPLICATION OF THE GHER 3D MODEL TO THE GENERAL SUMMER CIRCULATION IN THE NORTHERN BERING SEA

The Northern Bering Sea is a relatively shallow basin bounded by the Bering Strait to the north and St. Lawrence Island to the south (Fig. 5). The flow passing through the

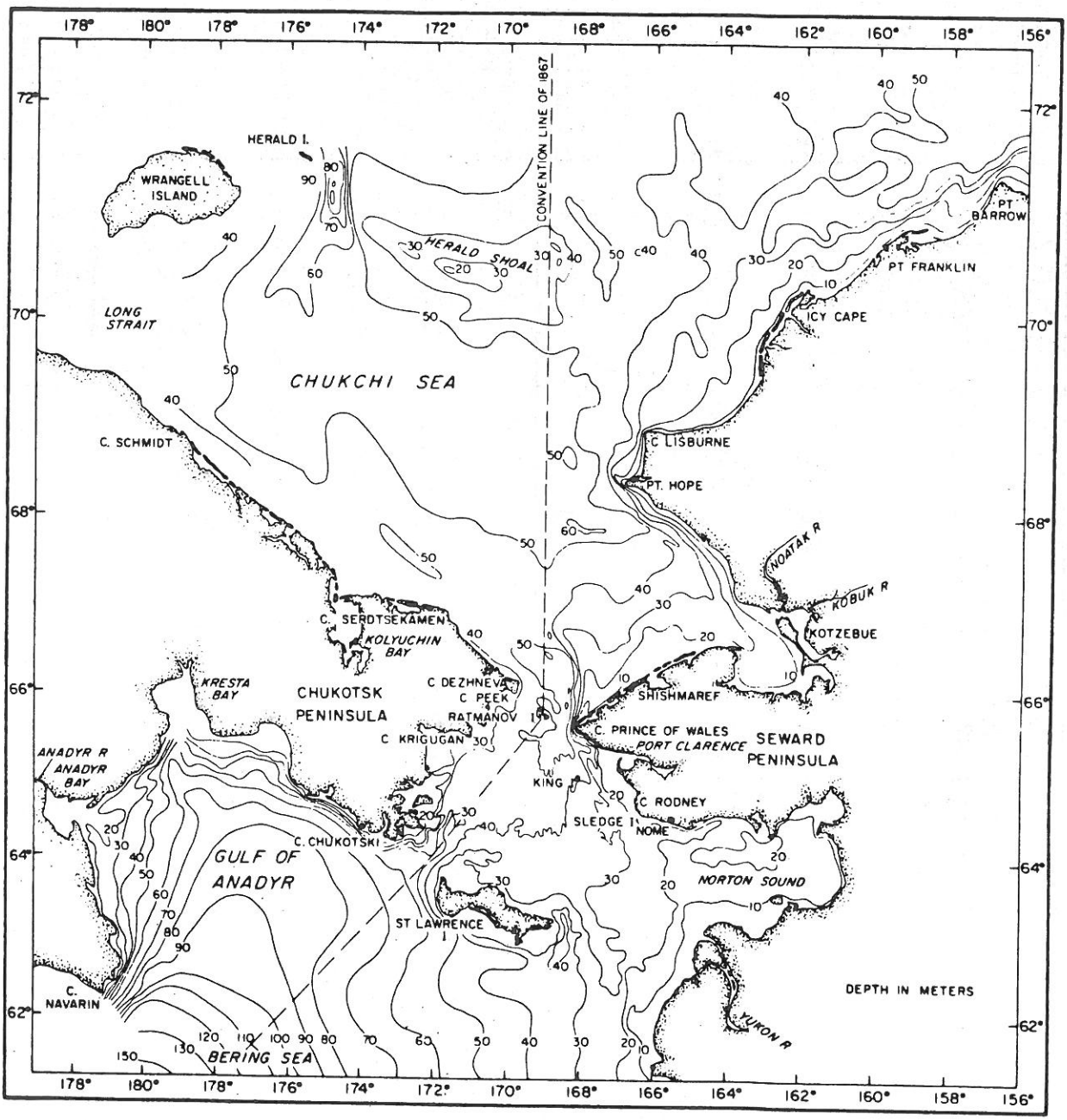


Fig. 5. The Northern Bering and Chukchi seas including Bering Strait.

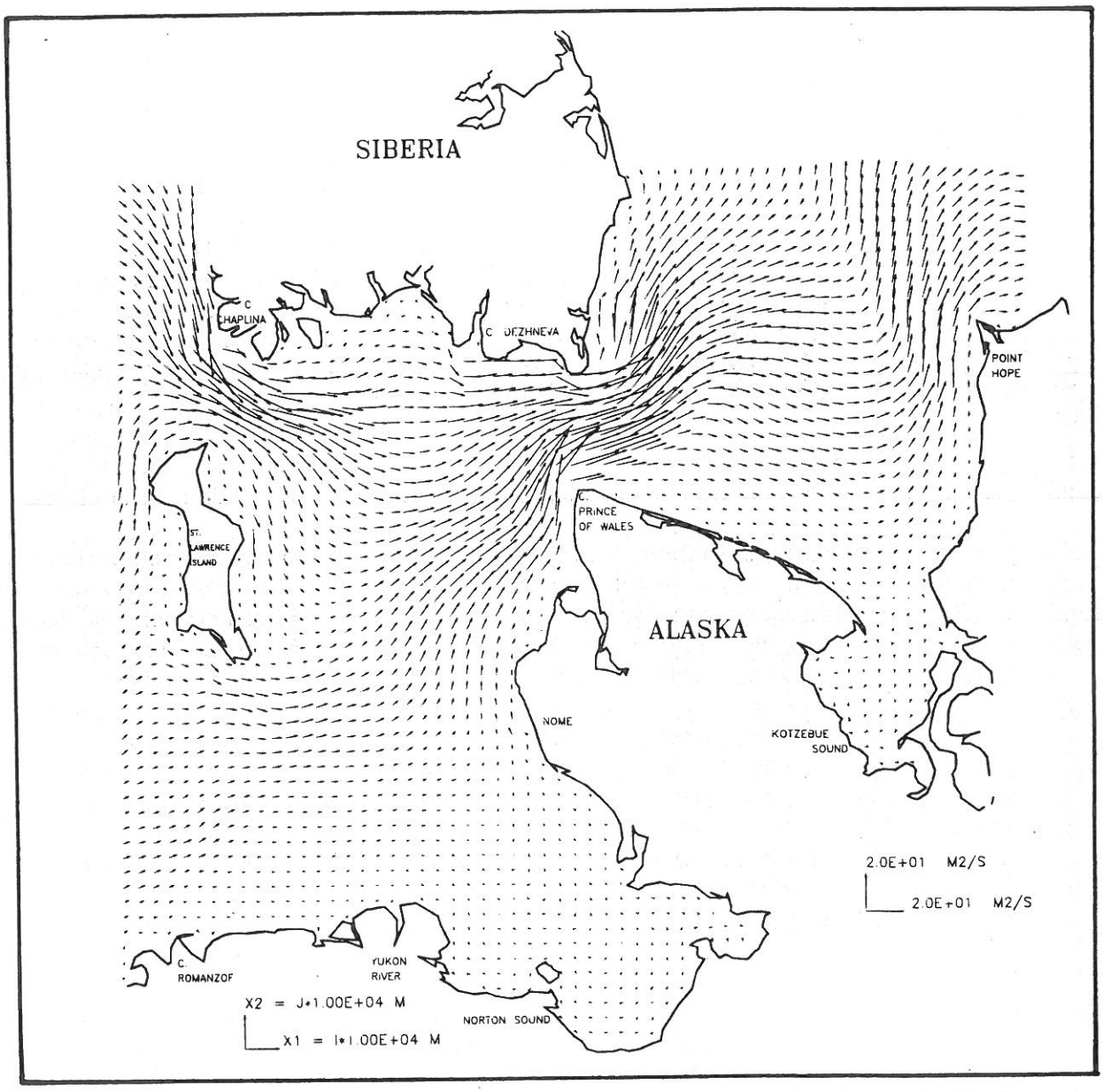


Fig. 6. General summer circulation in the Northern Bering Sea (1.8 Sv through Bering Strait). Total transport calculated by the 3D model ($m^2/s$). One can see the essential contribution of the "Anadyr Stream" flowing in through the Anadyr Strait (West of St. Lawrence Island) and deploying in the Northern Bering Sea.

Bering Strait, from the Pacific Ocean to the Arctic Ocean, penetrates the Northern Bering Sea through the Strait of Anadyr, to the west of St. Lawrence Island, and by the Strait of Shpanberg, to the east. More than 60% of the mean northward transport of water through the Bering Strait is derived from the "Anadyr Stream", a subsidiary of the Bering Slope Current which flows around the coasts of the Gulf of Anadyr, following the 60–70 m isobaths, to the Anadyr Strait and the western part of the Shpanberg Strait (Coachman et al., 1975). The proportion of that stream which goes through the Strait of Anadyr or skirts St. Lawrence Island, as well as the orientation and seasonal variations of the entering flow

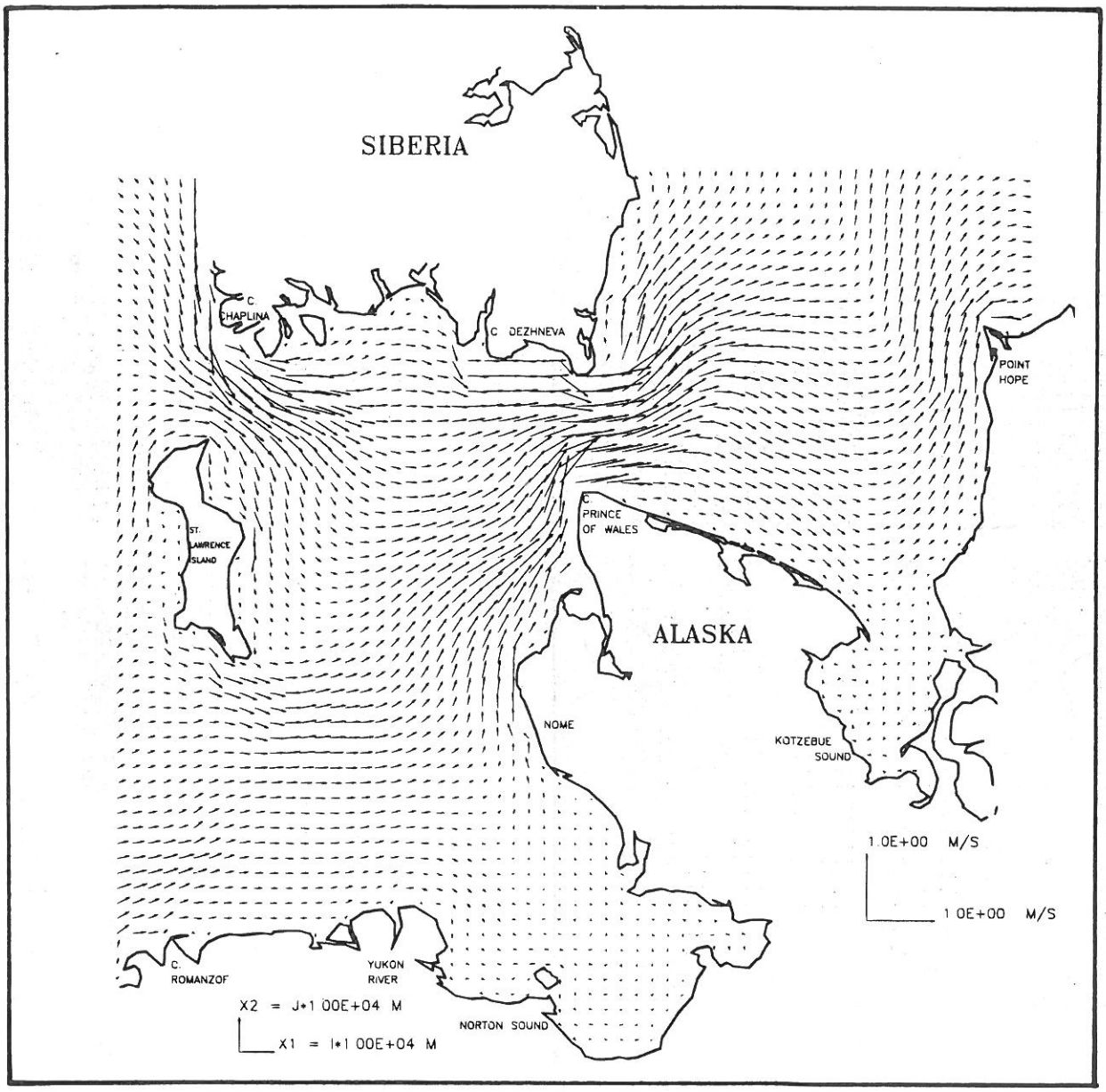


Fig. 7. General summer circulation in the Northern Bering Sea (1.8 Sv through Bering Strait). Current field at 5 m depth.

with respect to the Strait's axis, is likely to have a strong influence on the subsequent deployment of that flow in the Northern Bering Sea and in the Chukchi Sea.

Observations suggest that the Anadyr Stream is the main source of nutrients and biological productivity in the Northern Bering Sea (Walsh et al., 1985).

In preliminary studies for the ISHTAR NSF Research Project (e.g., Walsh et al., 1985), a series of numerical simulations was performed, with 2D barotropic and 3D baroclinic mathematical models, to test this hypothesis and determine if the general circulation pattern in the Northern Bering Sea was indeed compatible with observed biological data (Walsh and Dieterle, 1986; Nihoul et al., 1986).

The results of these exploratory simulations confirm the general trend of the Anadyr

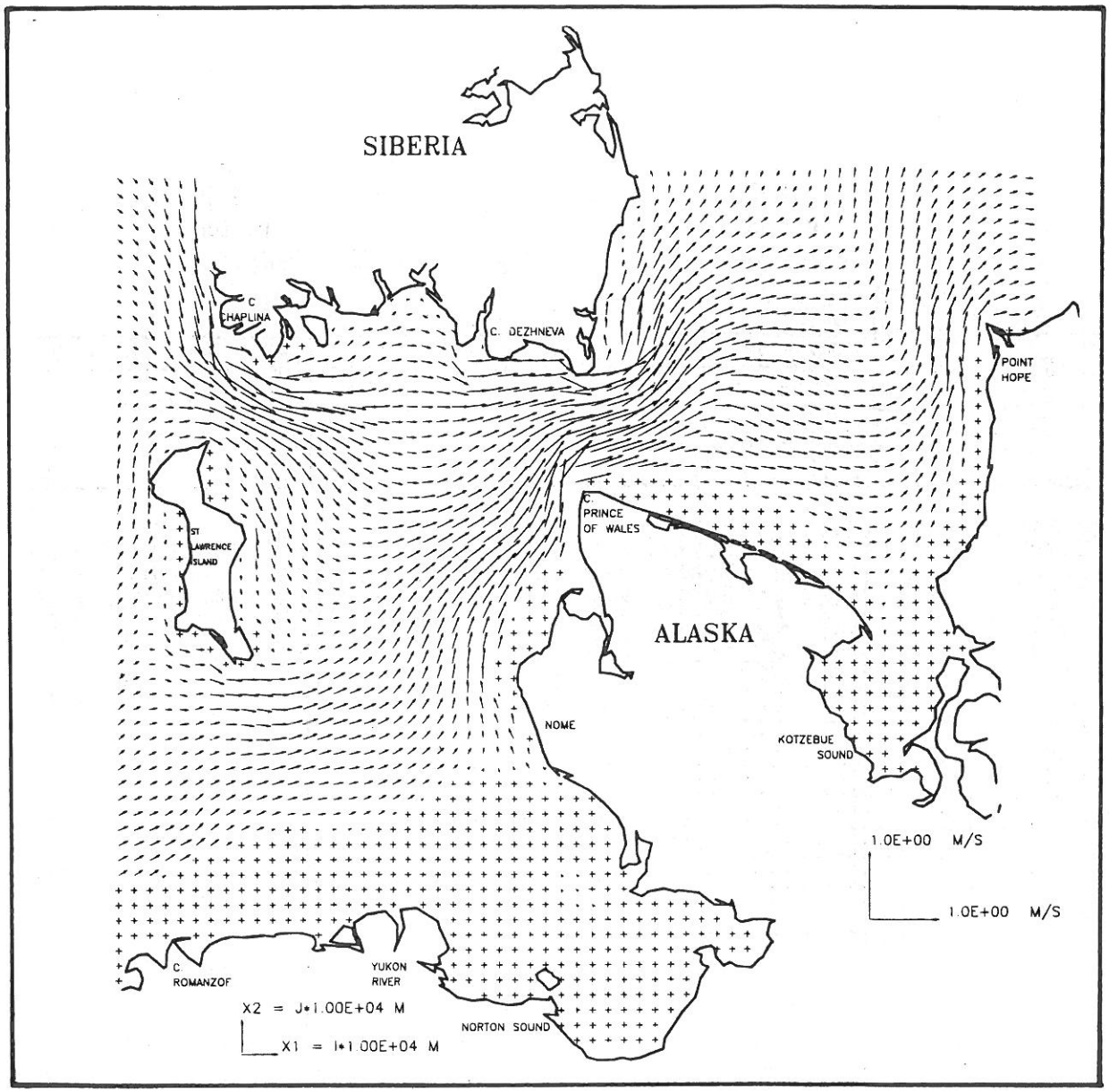


Fig. 8. General summer circulation in the Northern Bering Sea (1.8 Sv through Bering Strait). Current field at 20 m depth.

Stream to spread to the east after passing the Anadyr Strait, the nutrient-rich Anadyr waters deploying eastwards and progressively fostering biological productivity in the whole basin.

In subsequent developments of ISHTAR, experimental surveys and mathematical simulations were repeated over several years to assess the year-to-year variability of the system, with particular emphasis on the summer situation.

To gain a better understanding of the interannual variability, a preliminary simulation was made of a characteristic "climatic" summer circulation using initial and boundary conditions derived from historical data and representative of typical situations.

The result of this simulation provides a climatic reference to which subsequent simulations of the summers of '85, '86 and '87 can be compared. It also constitutes a perfect

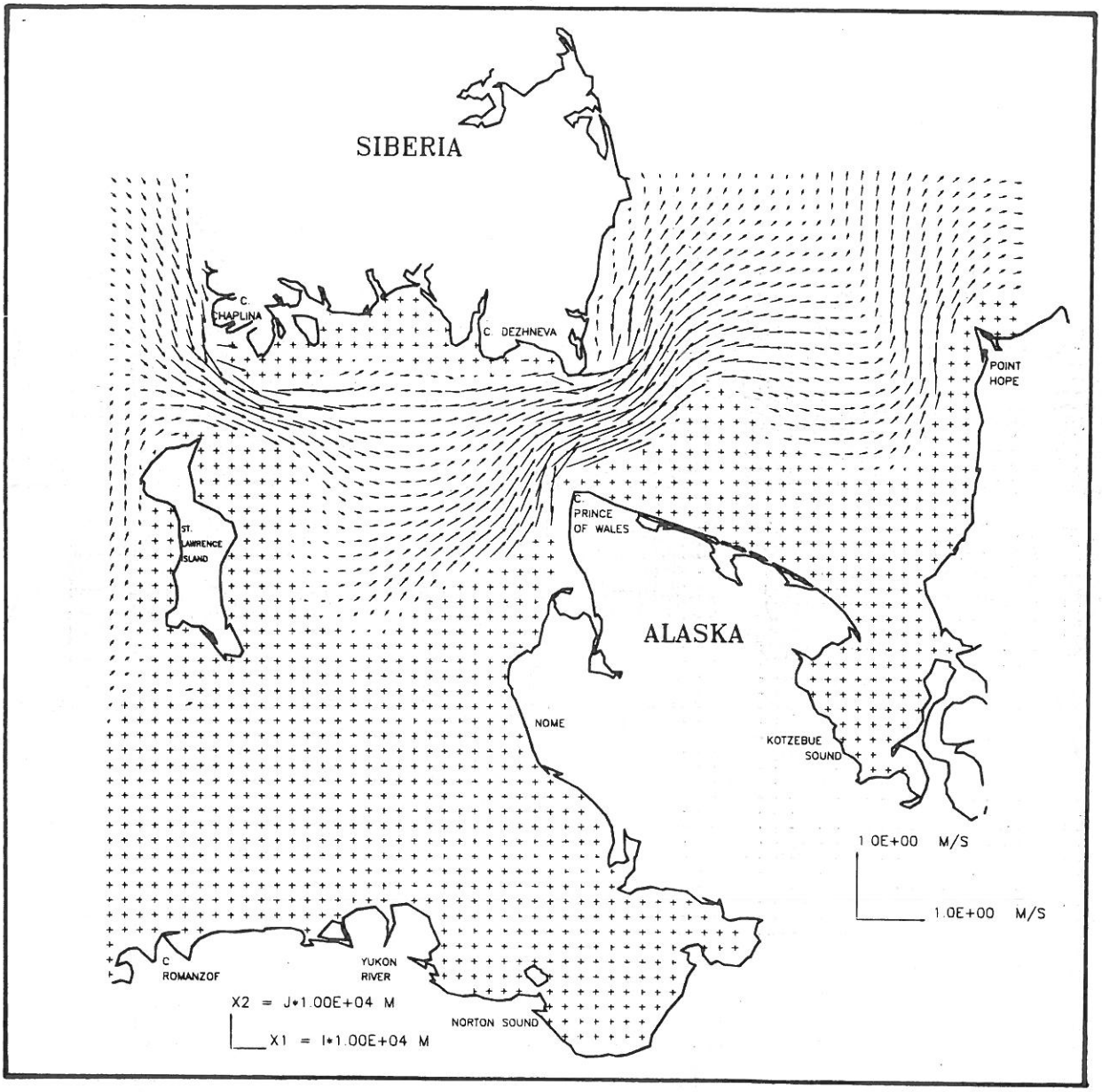


Fig. 9. General summer circulation in the Northern Bering Sea (1.8 Sv through Bering Strait). Current field at 35 m depth.

illustration of the application of the three-dimensional model to the study of the general circulation in shelf seas, the calibration of the model with historical data excluding the possibility of misleading good fortune with the reproduction of too specific data.

Some representative results of the "climatic" situation are shown in the following.

The model was calibrated and run with (initial and boundary) data typical of the summer season's climatology (Coachman et al., 1975). A total flow of 1.8 Sv was assumed through the Bering Strait. The flow was distributed along the southern boundary, ten grid points away from the limits of the Northern Bering Sea, according to observations and results from larger scale models. This resulted

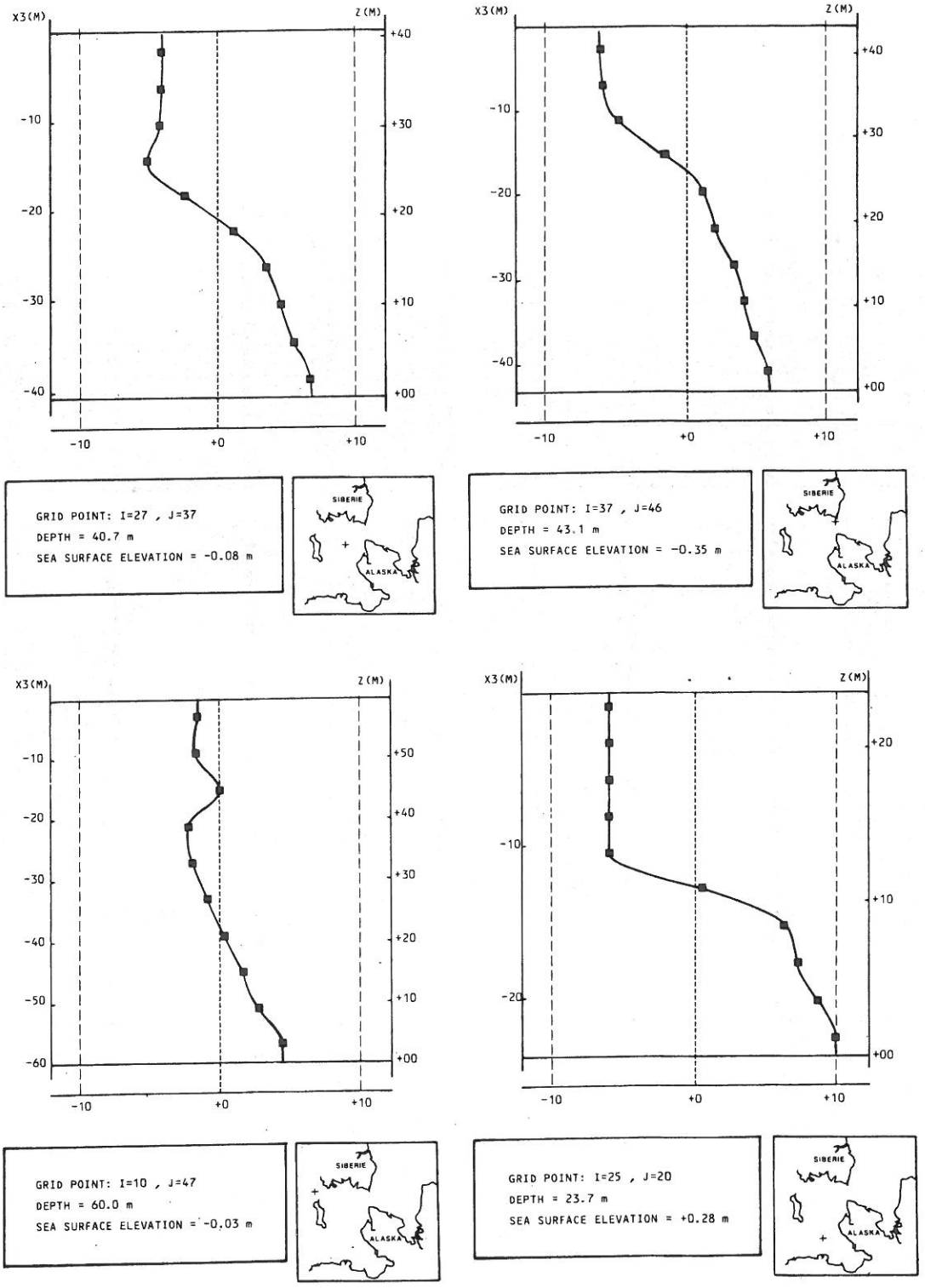


Fig. 10. Veering of the horizontal velocity vector at four locations in the Northern Bering Sea.

in a partition of inflows between the Anadyr Strait and the Shpanberg Strait in the ratio approximately two to one. The value of 1.8 Sv was derived from field measurements and actually interpolated between 1.9 Sv for a mean wind stress of $10^{-1}$ dyne $cm^{-2}$ north in early

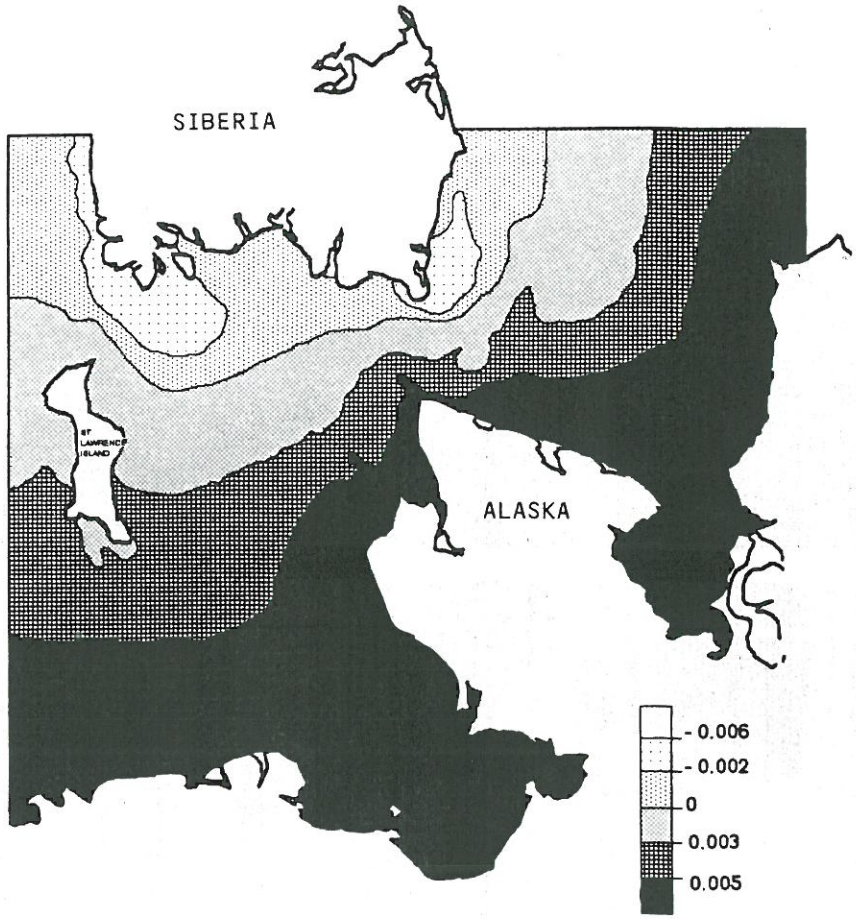


Fig. 11. General summer circulation in the Northern Bering Sea (1.8 Sv through Bering Strait). Buoyancy field at 5 m.

July 1968 and 1.7 Sv for a mean wind stress of the same order of magnitude south at the end of July 1972 (Coachman et al., 1975). The value of 1.8 Sv is not in itself a determinant factor of the general circulation pattern. At the general circulation scale, the residual non-linear advection terms are not dominant in the equations and the main effect of reducing or increasing the in-going transport is essentially a reduction or increase of the velocity scale although some localized discrepancies are not inconceivable (Nihoul et al., 1986).

Fig. 6 shows the total transport. One can see the essential contribution of the "Anadyr Stream" flowing in through the Anadyr Strait and deploying in the Northern Bering Sea in agreement with observations and previous studies. Figs. 7, 8 and 9 show the velocity field at 5 m, 20 m and 35 m depth, respectively. A relatively small but quite significant veering is apparent. The veering is exemplified in Fig. 10.

Figs. 11 and 12 represent the buoyancy field at 5 m and 15 m depth. Regions of upwelling (along the Siberian coast and the east coast of St. Lawrence Island) and regions of downwellings (along the Alaskan coast and the west coast of St. Lawrence Island) are marked respectively by large negative values at the surface and large positive values at depth. Vertical advection and mixing in the Anadyr Strait are illustrated by the cross-section distributions of buoyancy and turbulent kinetic energy shown in Fig. 13.

Horizontal distributions of buoyancy display non-negligible horizontal gradients and suggest the co-existence of different water

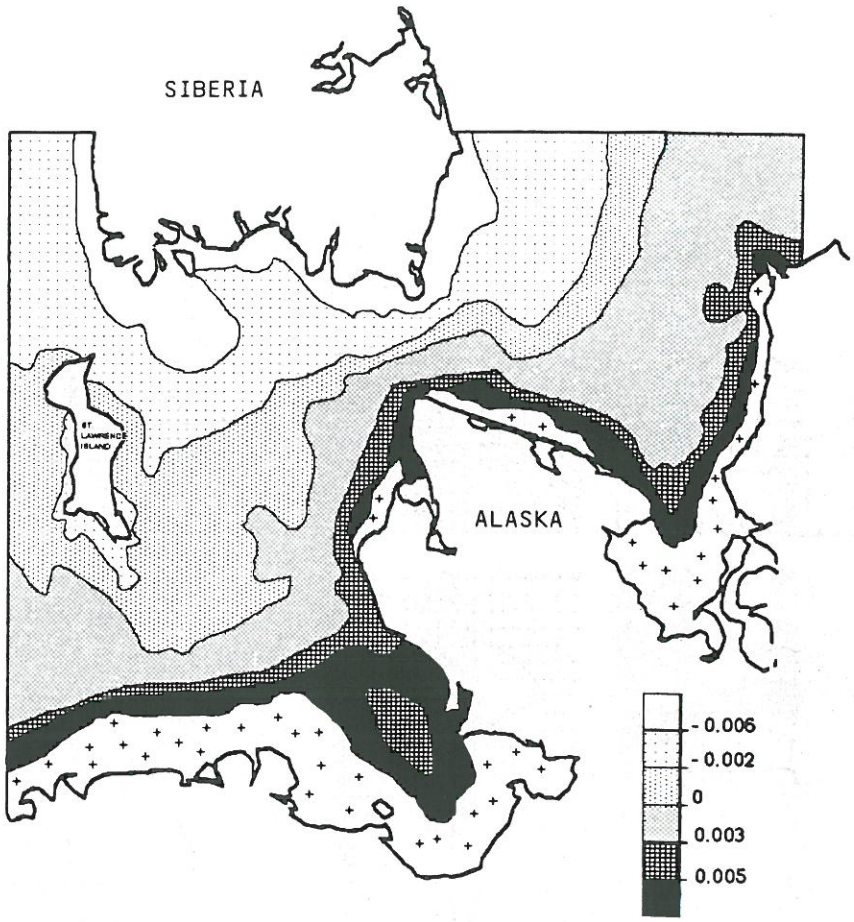


Fig. 12. General summer circulation in the Northern Bering Sea (1.8 Sv through Bering Strait). Buoyancy field at 15 m.

masses. Schematically, one can discern three regions: the Anadyr stream drawing along the nutrient-rich upwelled water of the Anadyr Strait into the Northern Bering and Chukchi seas, the Alaskan coastal waters filling the shallow eastern part and presumably overflowing the Anadyr Stream in the central region, an analogous riverine-influenced water mass off the Soviet coast denoted Siberian coastal water.

The separations between water masses have more or less pronounced frontal characteristics. The eastern front is the seat of occasional baroclinic instabilities giving rise to strong secondary flows in the form of eastwards propagating interleaving layers (Nihoul, 1986). These layers which have typically a width of 10 km in the early stages of development, widen progressively as they flow eastwards, spreading the nutrient-rich water over the Northern Bering Sea.

The formation of such layers can be explained by a baroclinic instability of the cold plume's frontal edge. Using the numerical results of the 3D model, the stability analysis gives the characteristics of the incipient layers in good agreement with the observations (Nihoul, 1986).

The occasional occurrence of a marked upwelling plume swept along in the Northern Bering Sea as an unstable frontal current and the subsequent development of extruding layers flowing eastwards, contribute, as the flow deployment described above, to the lateral diffusion of the nutrients and one may argue that the productivity of the Northern

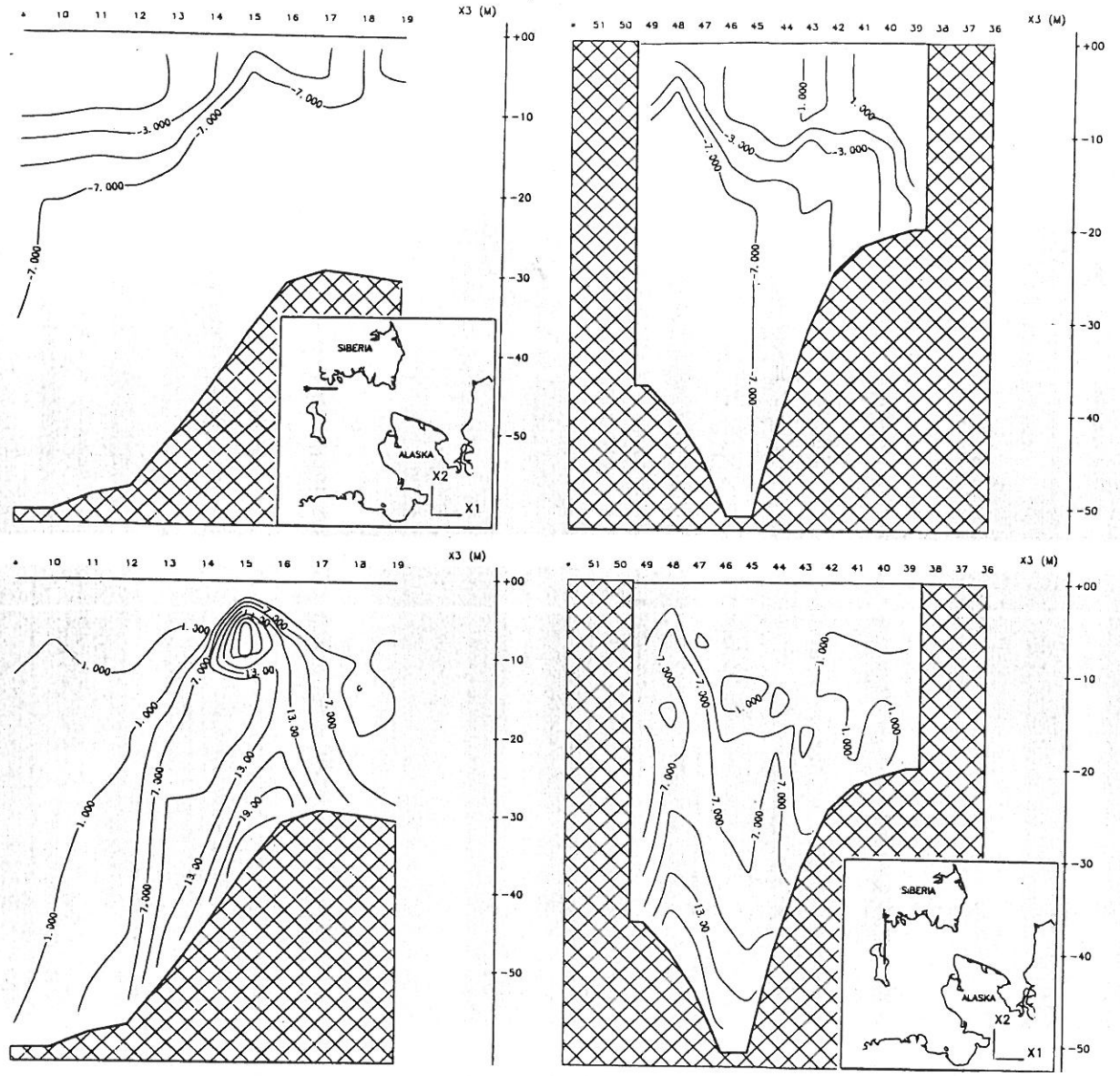


Fig. 13. Distribution of buoyancy (in $10^{-3}$ m $s^{-2}$) [above] and turbulent kinetic energy (in $10^{-4}$ $m^2$ $s^{-2}$) [below] in two perpendicular sections through the Anadyr Strait.

Bering Sea depends on the intensity and the variability of both the primary and secondary flows.

Experimental evidence of the Anadyr Strait upwelling, the "dateline" front and the synoptic interleaving layers is found in the remote-sensing images of the Northern Bering Sea (e.g., Fig. 14; Nihoul, 1986).

The examples presented above and all the other results of the climatic simulation (Deleersnijder and Nihoul, 1988) show a good agreement with both historical data and more recent observations made in the scope of the ISHTAR Program. The velocity and buoyancy fields, the partition of water masses, the vertical structures ... and the processes uncovered by the model such as upwellings, frontal instabilities ..., are confirmed by the data with everywhere the correct order of magnitude. (Small quantitative differences

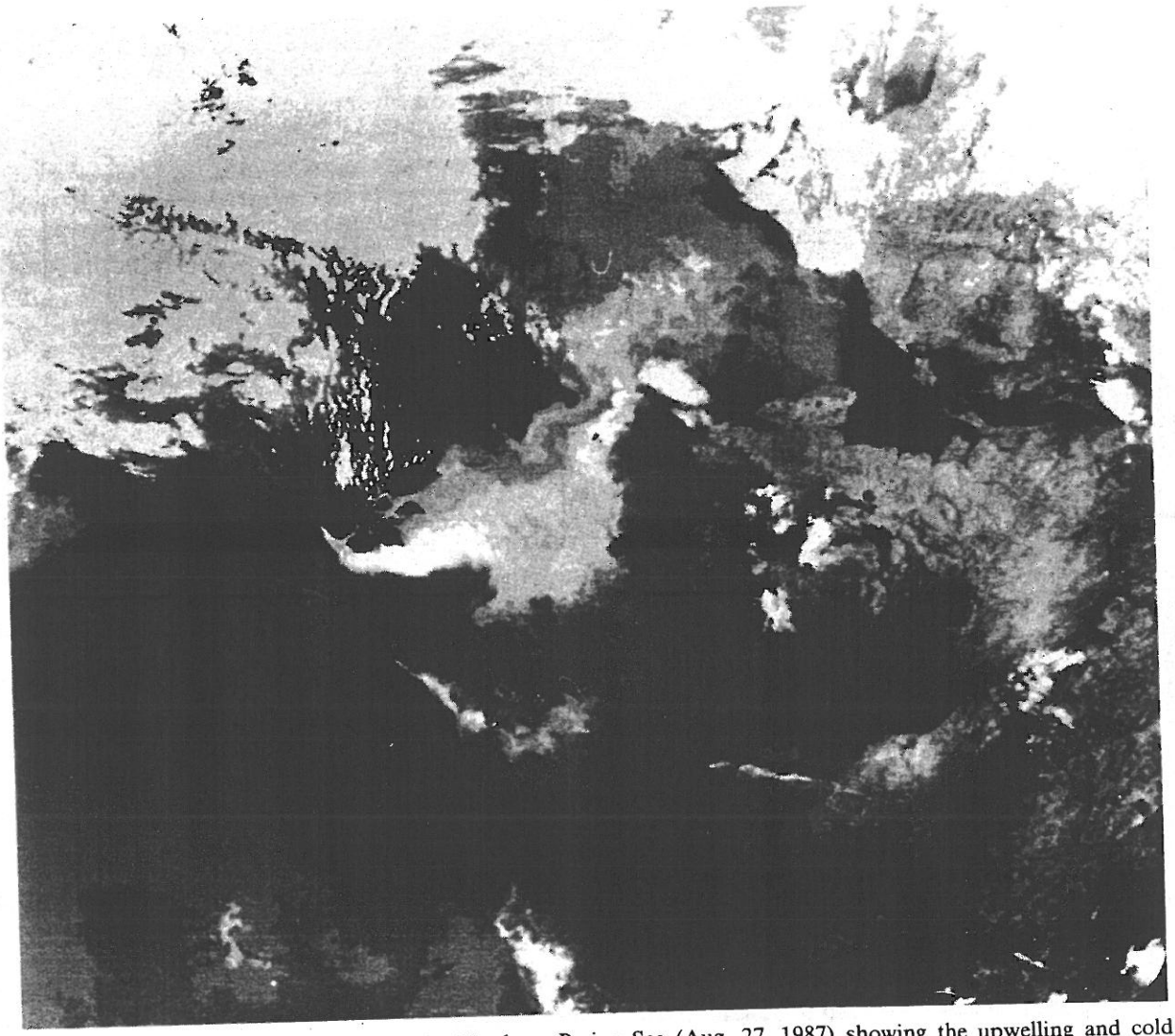

Fig. 14. Remote-sensing photograph of the Northern Bering Sea (Aug. 27, 1987) showing the upwelling and cold plume of nutrient-rich water coming up along the Siberian coast in the Strait of Anadyr and spreading northwards and eastwards under the action of the currents, with additional interleaving layers flowing to the east.

between the predictions of the climatic simulation and any particular set of measurements are in the range of anomalies of the natural variability of the system (e.g., Djenidi et al., 1988).)

This shows the reliability of the GHER GCM and provides an argument for the application of 3D $k$–$\epsilon$ models to the study of the general circulation.

## ACKNOWLEDGEMENTS

The authors acknowledge with gratitude the supports of the National Science Foundation (U.S.A.), of the Ministry for Science Policy (Belgium) and of the "Commissariat à l'Energie Atomique" (France). They are indebted to the National Fund for Scientific Research (Belgium) for providing supercomputer facilities.

## REFERENCES

Blumberg, A.F. and Mellor, G.L., 1980. A coastal ocean numerical model. In: J. Sündermann and K.P. Holz (Editors), Mathematical Modelling in Estuarine Physics. Springer Verlag, Berlin, pp. 203–219.

Blumberg, A.F. and Mellor, G.C., 1985. A description of three-dimensional coastal ocean circulation model.

In: N. Heaps (Editor), Three-dimensional Shelf Models, Coastal and Estuarine Dynamics, 5. American Geophysical Union Publ., pp. 1–16.

Coachman, L.K., Aagaard, K. and Tripp, R.B., 1975. Bering Strait. The Regional and Physical Oceanography. Univ. of Washington Press, Washington, 172 pp.

Deleersnijder, E. and Nihoul, J.C.J., 1988. General Circulation in the Northern Bering Sea. ISHTAR Annu. Progr. Rept., 392 p.

Djenidi, S., 1987. Modèles Mathématiques et Dynamique des Mers Continentales d'Europe Septentrionale. Ph. Dissertation, Liège University, 218 p.

Djenidi, S., Deleersnijder, E. and Nihoul, J.C.J., 1988. General Circulation in the Northern Bering Sea: Comparison of the results of the GHER 3D Model and the observation. AGU Ocean Sciences Meeting, New Orleans, 18–22 Jan., 1988.

Kitaigorodskii, S.A., 1979. Review of the theories of wind-mixed layer deepening. In: J.C.J. Nihoul (Editor), Marine Forecasting. Elsevier, Amsterdam, pp. 1–33.

Lumley, J.L., 1978. Computational modelling of turbulent flows. In: C.S. Yih (Editor), Advances in Applied Mechanics, 18. Academic Press, New York, N.Y., pp. 123–176.

Monin, A.S. and Ozmidov, R.V., 1985. Turbulence in the Ocean. Reidel, Dordrecht, 247 pp.

Monin, A.S., Kamenkovich, V.M. and Kort, V.G., 1977. Variability of the Oceans. Wiley, New York, N.Y., 241 pp.

Nihoul, J.C.J., 1975. Modelling of Marine Systems. Elsevier, Amsterdam, 272 pp.

Nihoul, J.C.J., 1977a. Modèles Mathématiques et Dynamique de l'Environnement. ELE, Liège, 198 pp.

Nihoul, J.C.J., 1977b. Three-dimensional model of tides and storm surges in shallow well-mixed continental seas. Dyn. Atmos. Ocean, 2: 29–47.

Nihoul, J.C.J., 1980. Marine Turbulence. Elsevier, Amsterdam, 378 pp.

Nihoul, J.C.J., 1982. Hydrodynamic Models of Shallow Continental Seas. E. Riga Publ., Liège, 198 pp.

Nihoul, J.C.J., 1986. Aspects of the Northern Bering Sea ecohydrodynamics. In: J.C.J. Nihoul (Editor), Marine Interfaces Ecohydrodynamics. Elsevier, Amsterdam, pp. 385–399.

Nihoul, J.C.J. and Djenidi, S., 1987. Perspective in three-dimensional modelling of the marine system. In: J.C.J. Nihoul and B.M. Jamart (Editors), Three-dimensional Models of Marine and Estuarine Dynamics. Elsevier, Amsterdam, pp. 1–34.

Nihoul, J.C.J., Waleffe, F. and Djenidi, S., 1986. A 3D-numerical model of the Northern Bering Sea. Environ. Software, 1: 1–7.

Rodi, W., 1980. Turbulence Models and Their Application in Hydraulics. IAHR Publ., Delft.

Rodi, W., 1987. Examples of calculation methods for flow and mixing in stratified fluids. J. Geophys. Res., 92: 5305–5328.

Walsh, J.J. and Dieterle, J., 1986. Simulation analysis of plankton dynamics in the Northern Bering Sea. In: J.C.J. Nihoul (Editor), Marine Interfaces Ecohydrodynamics. Elsevier, Amsterdam, pp. 401–428.

Walsh, J.J., Blackburn, T.H., Coachman, L.K., Goering, J.J., McRoy, C.P., Nihoul, J.C.J., Parker, P.L., Springer, A.M., Tripp, R.B., Whitledge, T.E. and Wirick, C.D., 1985. The role of the Bering Strait in carbon/nitrogen fluxes of polar marine ecosystems. Proc. Fairbanks Conf. Marine Living Systems of the Far North, May 1985.

[Received February 5, 1988; accepted May 27, 1988]